Spaceborne Synthetic Aperture Radar: Future Technologies and Mission Concepts

By Alberto Moreira, *Fellow IEEE*, Gerhard Krieger, *Fellow IEEE*, Michelangelo Villano, *Senior Member IEEE*, Marwan Younis, *Fellow IEEE*, Pau Prats-Iraola, *Fellow IEEE*, and Manfred Zink

ABSTRACT | This article provides an overview of the state-of-the-art and future developments in spaceborne synthetic aperture radar (SAR). Today, we are experiencing a golden age of spaceborne SAR, with the number of satellites in orbit increasing rapidly. This article presents novel technologies and mission concepts associated with innovative imaging modes, which are required to meet the stringent user requirements for improved performance, global coverage, faster revisit times, enhanced spatial resolution, and increased information content in SAR imagery. It is shown that key technologies and mission concepts, based on digital beamforming (DBF), bistatic and multistatic SARs, distributed SAR, and multiple-input multiple-output SAR (MIMO-SAR), will boost the performance and capabilities of the future generation of spaceborne SAR systems. In addition, this article addresses dedicated mission designs, technologies, and orbit concepts that are required to fulfill the specific user requirements. Two main streams in the spaceborne SAR development are presented alongside a tradeoff analysis: 1) NewSpace SAR, consisting of small satellites in the 85-kg to 250-kg weight class with the highest-resolution imagery and very short revisit times and 2) full-fledged SAR satellites with global coverage, high performance, and enhanced capabilities. It is shown that NewSpace and full-fledged SAR satellites are complementary in terms of user requirements, and that combining both mission concepts enables novel mission concepts, such as multistatic SAR, opening the door to a wealth of new applications. This article concludes with an outlook on the future of spaceborne SAR.

KEYWORDS | Bistatic and multistatic synthetic aperture radars (SARs); digital beamforming (DBF); distributed SAR; high-resolution wide-swath (HRWS); multibaseline imaging; NewSpace SAR.

I. Introduction

Spaceborne synthetic aperture radar (SAR) for Earth observation is unique in its capabilities: it is the only sensor technology that provides high-resolution imagery on a global scale, regardless of the weather conditions or daylight illumination [1], [2], [3], [4], [5]. While spaceborne optical sensors today provide images with a spatial resolution ranging from tens of meters down to a few decimeters, their imaging capability is limited by cloud cover and solar illumination. With an average global cloud cover of about 65% and a good sunlight window of about 4–6 h/day to avoid shadows, only ca. 6%–9% of the time is suitable for image acquisition [6]. In some areas of the world, like tropical forests, it may take up to a year to achieve a gapless coverage [7]. On the other hand, spaceborne SAR uses its own illumination, and the commonly used frequency bands from P (250–500 MHz), L (1–2 GHz), S (2–4 GHz), and C (4–8 GHz) to X (8–12 GHz)

Received 30 April 2025; revised 30 June 2025; accepted 28 September 2025.
(Corresponding author: Alberto Moreira.)
The authors are with German Aerospace Center (DLR), Microwaves and Radar Institute, 82234 Wessling, Germany (e-mail: alberto.moreira@dlr.de).

Digital Object Identifier 10.1109/JPROC.2025.3621586

are highly insensitive to cloud cover and rain. Fig. 1 shows typical examples of high-resolution SAR images of an urban area (top) and a medium-resolution wide-coverage image (bottom). While radar imagery contains complementary information to its optical counterpart, information retrieval from SAR imagery is more complex due to the interaction of microwaves with the Earth's surface.

Radar stands for radio detection and ranging. Space-based radars transmit high-power microwave pulses toward the Earth, and then, the echo signal is received, amplified by a low-noise amplifier, converted to baseband, and digitized. With the advances in digital technology, a direct signal digitization is today possible for frequencies up to the C band. By measurement of the echo signal, the so-called backscattered signal, a target detection, including its electrical and geometrical properties, is possible, while ranging is performed by measuring the time delay between transmission and reception. The intensity of each pixel in a radar image is a measure of the backscattered signal power and is commonly defined as sigma zero (or sigma nought), representing the radar cross section per unit area. This allows for comparisons between images from different radar systems, regardless of the spatial resolution of the image.

Both the amplitude and the phase in the radar image contain important information about the target's electrical and geometrical properties. Furthermore, the phase of the echo signal, scaled by the radar wavelength, is proportional to the distance between the radar antenna and the target. The phase information is also essential for applications based on SAR polarimetry and interferometry [3], [8], [9], [10]. For this reason, the SAR image pixels are commonly represented in a complex format with real and imaginary parts to preserve phase and amplitude information. Image intensity is simply the square of the modulus of each complex-valued pixel.

Basically, space-based radar can be divided into five different categories.

1) Radar altimeter, which estimates the topography of the oceans, ice sheets, or the Earth's surface with centimeter accuracy [4], [5], [11] by precisely measuring the time delay.
2) Scatterometer, a well-calibrated radar with coarse resolution that measures the backscatter intensity of the oceans and land surfaces to estimate wind speed and soil moisture, respectively [4], [5].
3) Cloud and precipitation radar, which uses higher frequency bands in the microwave spectrum, e.g., Ka band (26–40 GHz) or W band (75–110 GHz), to measure the intensity and type of precipitation and its dynamics.
4) Radar sounder, not yet flown in space for Earth observation but for planetary exploration, allows the measurement of the ice sheet thickness, the study of the subsurface geology, and the detection of subsurface features in arid regions using low-frequency bands [e.g., P band or very high frequency (VHF)] [12].
5) Spaceborne SAR, a high data rate, coherent radar with a side-looking geometry which provides a 2-D image of the Earth's surface.

SAR is by far the most complex type of space-based radar due to the requirements for: 1) high resolution, resulting in a high data rate; 2) phase and amplitude stability as well as calibration of the overall radar system; 3) coherence between successive radar pulses; 4) precise orbit knowledge and maintenance; and 5) the associated complex signal processing for image formation, which is usually performed on the ground after data downlink. A coherent radar system means that the phase information must be preserved for the formation of a synthetic aperture, a key step in the SAR imaging to achieve high resolution in the flight direction, as it will be explained later in Section II.

Although the invention of the SAR principle by Wiley [1] dates back to the 1950s, the first civilian spaceborne SAR, SEASAT (NASA/JPL) [13], was launched only in 1978, followed by ERS-1/2 (European Space Agency (ESA), 1991/95) [14], J-ERS-1 (Japanese Space Exploration Agency, JAXA, 1992) [15], and Radarsat-1 (Canadian Space Agency, CSA, 1995) [14]. A milestone in this early phase of spaceborne SAR was set by several shuttle imaging radar (SIR) missions, most notably, SIR-C/X-SAR (NASA/JPL, DLR, and ASI, 1994) and Shuttle Radar Topography Mission (SRTM, NASA/JPL, DLR, and ASI, 2000) [16]. While SIR-C/X-SAR was the first multifrequency and polarimetric SAR in space, demonstrating a number of novel technologies, imaging techniques, and applications, SRTM was the first dedicated single-pass interferometric SAR mission to generate a global topographic map of 80% of the land masses. SRTM rapidly became a reference for numerous geoscience and geospatial applications, as well as the basis for a number of subsequent topographic mapping products. Newer datasets based on SAR interferometry, such as TanDEM-X, offer improved resolution and accuracy and are already providing the next generation of topographic mapping products. With the launch of TerraSAR-X [17], COSMO-SkyMed [18], and Radarsat-2 [19], civilian SAR systems began providing images with a resolution of 1 m and even less for the first time. Later in 2010, TanDEM-X set a further milestone in the spaceborne SAR development with the first interferometric SAR mission consisting of two satellites flying in close formation [20]. Within the ESA/EU Copernicus program, a successful series of Sentinel-1 radar satellites was established in 2014, providing dual-polarized C-band data with open access [21]. Currently, Sentinel-1A and Sentinel-1C are operational, and Sentinel-1D was launched in November 2025. In 2018, a paradigm shift in spaceborne SAR occurred with the development of disruptive concepts and technologies for small satellites in the 85–250-kg class, enabling a business case to be established. This class of privately funded satellites is referred to as NewSpace SAR and is described in Section IV. NewSpace SAR, largely funded by private investment and venture capital, is based on a constellation of small satellites that

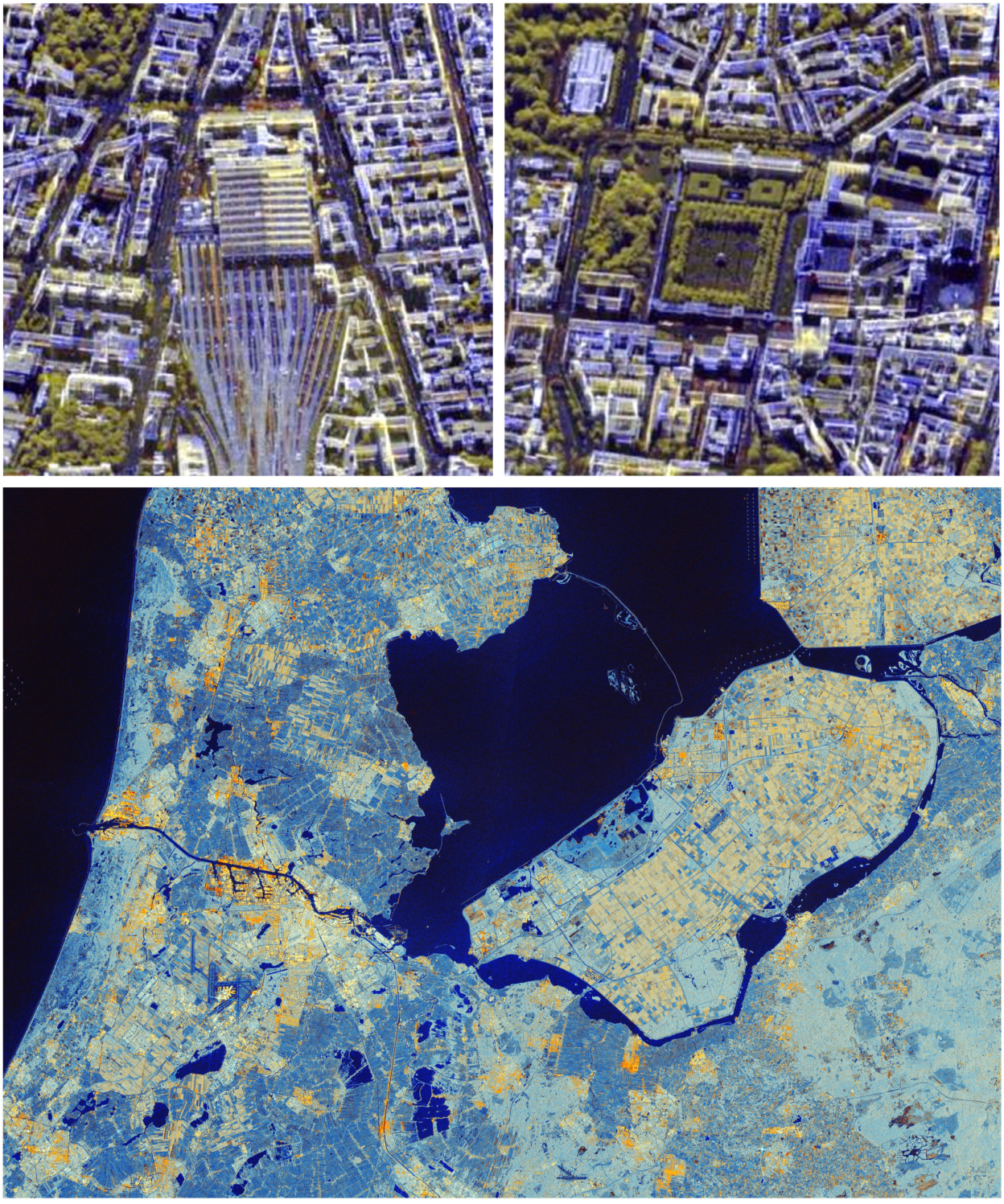

Fig. 1. ***Zoomed-in view of a high-resolution SAR image of Munich's main railway station and the courtyard of Munich Residence, respectively, acquired by the TerraSAR-X satellite (resolution: 25 cm $\times$ 1 m and image size: 800 $\times$ 800 m) (top left and right). One of the first images of the ESA/EU Copernicus Sentinel-1C satellite launched in December 2024, showing Amsterdam and the Flevoland region, The Netherlands (resolution: 5 $\times$ 20 m, image size: 100 $\times$ 75 km, and image credit: ESA) (bottom). In all cases, a pseudo-color image representation was used to improve image interpretation. Overlay of a series of 15 co-registered images: man-made targets (bluish), vegetation (green), and changes between images (reddish, e.g., trains on the track) (top left and right). Colors are associated with different polarizations: HH (bluish) and HV (reddish), where HH stands for horizontal transmit and receive, and HV stands for horizontal transmit and vertical receive (see Section II) (bottom).***

enable revisit times of a few hours, thereby addressing new business cases that have not been possible by full-fledged SAR systems.

A spaceborne SAR system typically flies in a polar orbit at an orbit altitude of 500–800 km. Other orbital concepts are required for specific applications, as it will be discussed in Sections II, IV, and V. Adding a second antenna at the tip of a boom (as for SRTM) or a second SAR satellite at a distance of, e.g., a few hundred meters (as for TanDEM-X), enables 3-D imaging by using the principle of radar interferometry, i.e., the phase difference received by different antennas is used to provide accurate information about the surface elevation. Using multiple antennas with a physical separation, called baseline, allows not only for SAR interferometry [8], but also for SAR tomography or even holographic SAR tomography, as it will be described in Section V. In the case of interferometric acquisitions with a temporal baseline (i.e., a time lag of days to decades between image acquisitions), the phase information can be used to estimate the target displacement (i.e., ground deformation) with an accuracy down to a millimeter. This technique is referred to as differential SAR interferometry [9] and is also described in Section V.

The range of applications for SAR imagery is rapidly expanding and includes the following:

1) environmental monitoring (e.g., land cover mapping, crop- and forest-type classification, and natural resource management);
2) hazard monitoring (e.g., oil spill, landslide, flood, earthquake and volcano monitoring, and disaster response);
3) urban, infrastructure, and traffic monitoring;
4) geoscientific research (e.g., soil moisture estimation, permafrost extent and change, wetland monitoring, forest biomass, snow cover, snow water equivalent, ice and glacier cover, and its velocity);
5) archeology (e.g., Angkor Wat and Oman [22]);
6) climate change studies;
7) 3-D mapping;
8) change detection from image time series;
9) subsidence monitoring;
10) ocean applications (e.g., ocean currents, wind speed over sea surface, coastal bathymetry, and sea state);
11) reconnaissance and security applications.

Spaceborne SAR also plays an important role in planetary exploration, as in the case of Magellan (NASA/JPL, 1989, which imaged the Venus' surface with a resolution of ca. 300 m [23]) and Cassini (NASA/JPL, 1997, which studied the surface of Saturn's moon Titan [24]). In both cases, the dense atmosphere is not transparent to optical sensors, making SAR the only sensor capable of high-resolution imaging. SAR systems for planetary observations have stringent requirements regarding data transmission to the Earth, radiation hardness, thermal control, power availability, mass and space constraints, etc. As a result, the SAR instrument concepts are much simpler, and the complexity of the imaging modes is far less than that developed for Earth observation. Therefore, this article will focus on technologies and mission concepts for Earth observation although many of the ideas can be applied to planetary exploration.

This article provides an overview of future spaceborne SAR technologies and mission concepts. Section II introduces the SAR principles, including the constraints on the SAR system design. It also summarizes the various imaging modes and describes the user requirements for future satellite SAR missions. It concludes with a summary of the state of the art. Section III provides an overview of advanced SAR instrument architectures and describes the paradigm shift occurring in the development of SAR systems: digital beamforming (DBF) allows for the implementation of innovative imaging modes with high azimuth resolution and wide swath coverage, thus circumventing the fundamental design limitation of conventional SAR systems. DBF means moving from an analog phased array antenna toward a multichannel antenna with multiple digital receive channels. Section IV provides an insight into NewSpace SAR: a game changer in the SAR development that enabled the realization of constellations with a large number of SAR satellites. Section V introduces bistatic and multistatic SAR imaging, which enables a wealth of new information products to be generated from SAR imagery. Furthermore, the concept of distributed SAR opens the door to very powerful SAR system configurations using small satellites. Section VI concludes this article by showing that full-fledged SAR and NewSpace SAR systems are complementary and will pave the way for future spaceborne SAR development. This section also highlights the need for different and innovative SAR system and instrument concepts to address a variety of user requirements.

II. SAR BASICS AND STATE OF THE ART

A. SAR Basics and Design Constraints

In this section, a concise description of the SAR basics and state of the art is presented. Detailed descriptions and mathematical derivations can be found in several sources [2], [3], [4], [25], [26], [27], [28].

A conventional spaceborne SAR system consists of a radar embarked on a satellite platform, typically following a sun-synchronous low-Earth orbit (LEO). It operates by transmitting periodically electromagnetic pulses to the Earth and receiving and storing onboard the corresponding echoes. These raw data are downlinked afterward to the ground, where they are processed digitally to obtain the SAR image. The radar antenna illuminates boresight to the motion direction and looks to one side of the ground track in order to avoid the ambiguous reception of undesired signals coming from the opposite side. The capability to distinguish targets along range is determined by the range spatial resolution of the system, as depicted in the left image of Fig. 2. Being a radar, the targets appear in the final image depending on the sensor–target

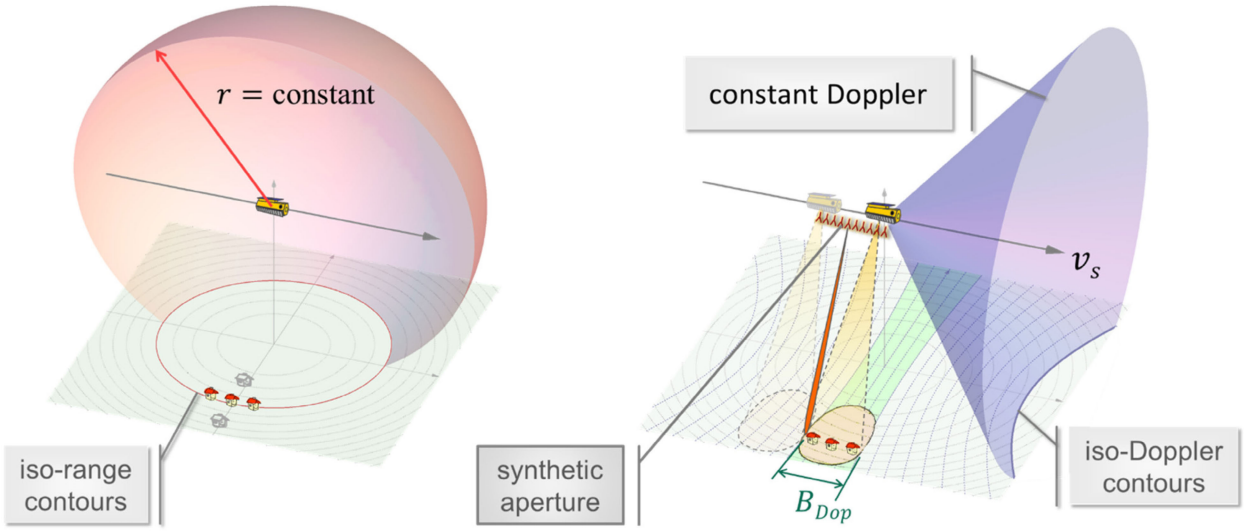

Fig. 2. ***Basic SAR imaging geometry and resolution: (a) radar range measurement and (b) range–Doppler measurement. The red circle on the left highlights one iso-range contour as the intersection of the red sphere and the ground for a particular range. The three targets on the ground are located on this contour, meaning that they are at the same distance from the radar. In order to discriminate targets at the same range distance, the Doppler effect is exploited. The iso-Doppler contours on the right show the targets on the ground experiencing the same instantaneous Doppler frequency. The Doppler cone represented in magenta intersects the ground with the shape of a hyperbola. The intersection of the iso-range and iso-Doppler contours determines the final resolution cell.***

distance, i.e., the target position is determined by measuring the time delay between transmission and echo reception. Frequency-modulated pulsed waveforms, called chirps, are typically used in radar systems in order to achieve a high spatial resolution [4]. They provide a good compromise between resolution and transmitted power efficiency, requiring a pulse compression step during the SAR image formation process. This processing step is typically performed on the ground via a matched filter operation either in the time or frequency domain [29]. After the pulse compression, the range resolution is given by

$$\delta_r = \frac{c_0}{2 \cdot B_{\mathrm{rg}}} \tag{1}$$

where c_0 is the speed of light and B_{rg} is the bandwidth of the transmitted pulse.

The second dimension in the slant-range plane is the so-called azimuth dimension and is aligned with the motion vector of the platform. The right image of Fig. 2 depicts how the SAR system achieves a high spatial resolution in the azimuth dimension by means of exploiting the Doppler effect. A given target on ground experiences an almost linear variation of the instantaneous Doppler frequency during the observation time. Due to this frequency variation, the received signal in azimuth is approximately described by a chirp as well although its time duration can be a few 100 ms to tens of seconds in the case of submetric azimuth resolution. Similar to the range dimension, the processing is performed on ground via matched filtering. Note that the SAR image formation process has been presented here in a simplified way, but in practice, it requires the implementation of complex signal processing algorithms to consider several factors, like the variation of the range distance to each target during the observation time and the coupling between the range and azimuth chirps, to achieve a properly focused SAR image [27], [28], [29], [30], [31]. A paramount requirement for azimuth compression is that the radar system has to be *coherent*. This requirement implies that the phase information of the received signals, which is proportional to the two-way distance between the targets in the scene and the radar antenna, must be preserved from pulse to pulse. In conventional monostatic SAR systems, this is achieved by using ultrastable oscillators (USOs). Due to its challenging aspects in bistatic and multistatic SAR systems, synchronization is a system design driver, as will be discussed in Section V.

Due to the coherent nature of the transmitted electromagnetic signal, the received echo from a single resolution cell includes the sum of the backscattered echoes of all elementary scatterers inside this cell. For a distributed scatterer, such as a crop field or forest, there may be tens to thousands of elementary scatterers in a resolution cell, depending on the wavelength and the spatial resolution of the SAR system. The sum of all these responses, which depends on the spatial distribution and electromagnetic properties of the single scatterers, is, therefore, random and varies from pixel to pixel. This effect results in a salt-and-pepper-noise-like pattern in the SAR image called *speckle* [2], [3], [4], [25], [26], [27], [28]. Speckle is inherent to coherent measurements and makes the image difficult to interpret. To mitigate this,

spatial averaging of the intensity image, denoted as multilooking, is typically applied, resulting in a loss of spatial resolution [2], [3].

In the following, the azimuth spatial resolution of a SAR system is derived from the Doppler point of view. Considering an antenna with a uniform intensity distribution, its 3-dB beamwidth, i.e., the angular width of the main beam at half of the maximum power, is approximately given by

$$\theta_{3\ \mathrm{dB}} = k \cdot \frac{\lambda}{l_a} \tag{2}$$

where $0.8 \leq k \leq 2$ depending on antenna type and design, λ is the wavelength, and l_a is the physical length of the antenna in the azimuth dimension. Using the Doppler relation between instantaneous frequency and motion, the total Doppler bandwidth observed through the 3-dB beamwidth corresponds to

$$B_{\mathrm{Dop}} \approx \frac{2 \cdot v}{l_a} \tag{3}$$

where v is the spacecraft velocity. The azimuth resolution in meters is, therefore, given by

$$\delta_{\mathrm{az}} = \frac{v}{B_{\mathrm{Dop}}} \approx \frac{l_a}{2} \tag{4}$$

where the approximation on the right-hand side of the equation, commonly used in the literature, indicates that the final azimuth resolution approximates half of the physical antenna size in the azimuth dimension. The final size of the resolution cell is determined by the intersection of the iso-range and iso-Doppler contours, as depicted in Fig. 2. Please note that the image formation in the azimuth direction can also be understood as the synthetization of a long antenna in azimuth, the length of which is defined by the illumination time (see Fig. 2, right). Since the length of the synthetic aperture increases linearly with range, the azimuth resolution is independent of the range distance.

Besides the spatial resolution, there are other image quality metrics that need to be considered, and which impose requirements on the radar instrument design and operation. One such metric is the peak-to-sidelobe ratio of the compressed pulse, which can be suppressed to typically -30 dB by introducing a weighting function into the matched filter. Another metric is related to the so-called ambiguities [32]. Due to the finite size of the physical antenna, both in the azimuth and elevation dimensions, energy is transmitted outside of the desired directions through the antenna sidelobes. This energy bounces back from the imaged scene and can result in undesired artifacts in the final focused image, thus potentially degrading the image quality. In general terms, the ambiguity-to-signal ratio is defined as the ratio of integrated energy received by the antenna from undesired angular directions to the integrated energy coming through the angles of interest. This ratio should ideally be small, being better than -20 dB in current SAR systems. The mechanism through which ambiguities arise is different depending on the radiation direction of the antenna under consideration, and therefore, the SAR community typically differentiates between azimuth and range ambiguities.

Let us address the azimuth ambiguities first. By means of periodically transmitting pulses and receiving the corresponding echoes, a SAR system samples the azimuth spectrum of the scene, which, through the radar operation, is weighted by the azimuth antenna pattern. The sampling occurs at a rate given by the pulse repetition frequency (PRF). Therefore, signals with an instantaneous Doppler within $\pm$PRF/2 will be properly sampled, whereas signals with a larger instantaneous Doppler will be insufficiently sampled and result, consequently, in *aliasing*. As indicated before, a finite-sized antenna transmits and receives energy through its main lobe and sidelobes with a radiation pattern that depends on the antenna architecture. A rectangular aperture, for example, exhibits a sinc-like azimuth antenna pattern, as depicted in the left image of Fig. 3. In this example, the PRF has been selected such that most of the signal bandwidth observed through the main beam, which is depicted in green, is properly sampled. However, the Doppler signals beyond $\pm$PRF/2, depicted in red, will result in azimuth ambiguities. The small gaps depicted in gray do not contribute to the main signal nor to the ambiguous signals. They represent the fact that the raw data processor usually limits the azimuth processed bandwidth, or in other words, the Doppler bandwidth required to achieve the desired azimuth resolution is generally smaller than the PRF. For this reason, those samples are set to zero in the Doppler spectrum by the processor.

The image formation process will properly focus the energy of those signals within the unambiguous interval of $\pm$PRF/2. The aliased signals, on the other hand, will be focused as if they were legitimate signals—the name *ghost* is also used to describe them. However, they will appear in the image displaced in the azimuth direction from the actual location of the true target, potentially masking the actual legitimate signal at that location. Azimuth ambiguities can be clearly observed in scenes with a very heterogeneous backscatter, e.g., land areas next to water bodies. The right image of Fig. 3 shows an example of azimuth ambiguities with a TerraSAR-X acquisition along the coast of Catalonia, Spain, which was acquired with a purposely low PRF value to increase the level of the azimuth ambiguities. A ghost image overlaying on the sea can be clearly observed along the entire coast. Similarly, strong targets surrounded by a low clutter signal tend to result in clearly visible azimuth ambiguities, like the ship highlighted in the top right of Fig. 3.

SAR systems are designed to sample the 3-dB azimuth antenna beamwidth, i.e., the PRF must be larger than the Doppler bandwidth required to achieve the desired azimuth resolution of the system. As noted above, the total Doppler bandwidth observed at the 3-dB beamwidth

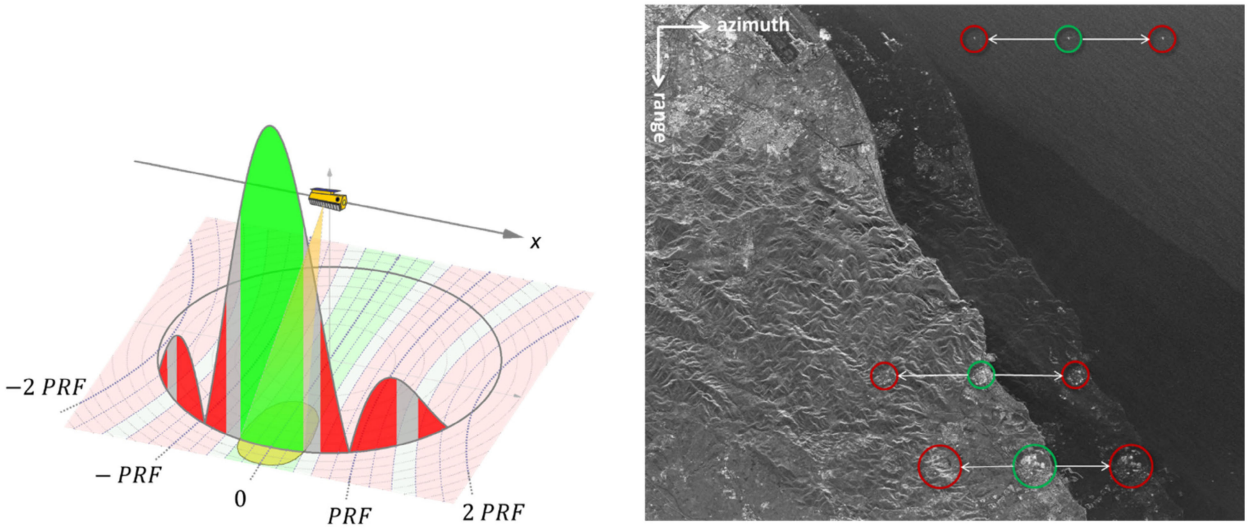

Fig. 3. *Azimuth ambiguities in SAR systems. The image on the left depicts how azimuth ambiguities arise since the azimuth signal is not band-limited. Signals with an instantaneous Doppler frequency beyond ±PRF/2 are not properly sampled and result in ghost responses in the final image, potentially degrading its quality and interpretability. The right image shows an extreme example of azimuth ambiguities, where the PRF was purposely set too close to the 3-dB beamwidth of the antenna.*

of the antenna is given by (3). Therefore, this Doppler bandwidth at 3 dB corresponds indeed to the minimum PRF with which the radar system should operate. In the SAR community, this minimum PRF is also referred to as the Nyquist frequency for the azimuth signal. In order to meet Nyquist, successive pulses must be sent at time intervals, in which the sensor moves by approximately half the azimuth antenna length. However, a system operating at this minimum PRF, or close to it, would still result in large azimuth ambiguities.

In order to mitigate the impact of azimuth ambiguities, one could consider using a PRF larger or even much larger than the 3-dB Doppler bandwidth. However, the PRF also has an impact on the size of the imaged swath. Indeed, the swath width will be inversely proportional to the system PRF. During operation, the timing sequence of the spaceborne SAR system is designed in such a way that it is either transmitting a pulse or receiving the echoes, so that the swath width is as large as possible for a given PRF value. Consequently, the duration of the receive echo window, which defines the size of the swath, is limited by the pulse repetition interval (PRI), the inverse of the PRF. The maximum swath on ground is approximately given by

$$SW_{\max} \approx \frac{c_0}{2 \cdot \mathrm{PRF} \cdot \sin\theta_i} = \frac{c_0 \cdot \mathrm{PRI}}{2 \cdot \sin\theta_i} \tag{5}$$

where θ_i is the incidence angle in the middle of the illuminated swath. The incidence angle is defined as the angle between the radar beam and the local surface normal at a given position on the swath. θ_i typically varies from 20° (at the near range) to 50° (at the far range). Note that this equation neglects the time during which the radar transmits the pulse, typically in the order of 30–50 μs in spaceborne systems. Equations (3)–(5) provide, respectively, the minimum and maximum values a SAR system should consider for the PRF. They represent one of the main tradeoffs in the design of SAR systems, namely, that the imaged swath is proportional to the azimuth resolution of the system, i.e., a fine spatial resolution implies a small swath. This tradeoff is also known as the SAR system design dilemma and is depicted in Fig. 4.

Fig. 4 also indicates the impact of range ambiguities, which are addressed in the following. As mentioned before, energy is transmitted and received through the sidelobes of the elevation antenna pattern, which illuminate areas beyond the desired swath. This energy bounces back to the radar and overlaps with the echoes received

Fig. 4. *SAR system design dilemma for conventional SAR systems, showing the main tradeoff between swath width and azimuth resolution. The table depicts typical tradeoffs between azimuth resolution and swath width for a spaceborne SAR system.*

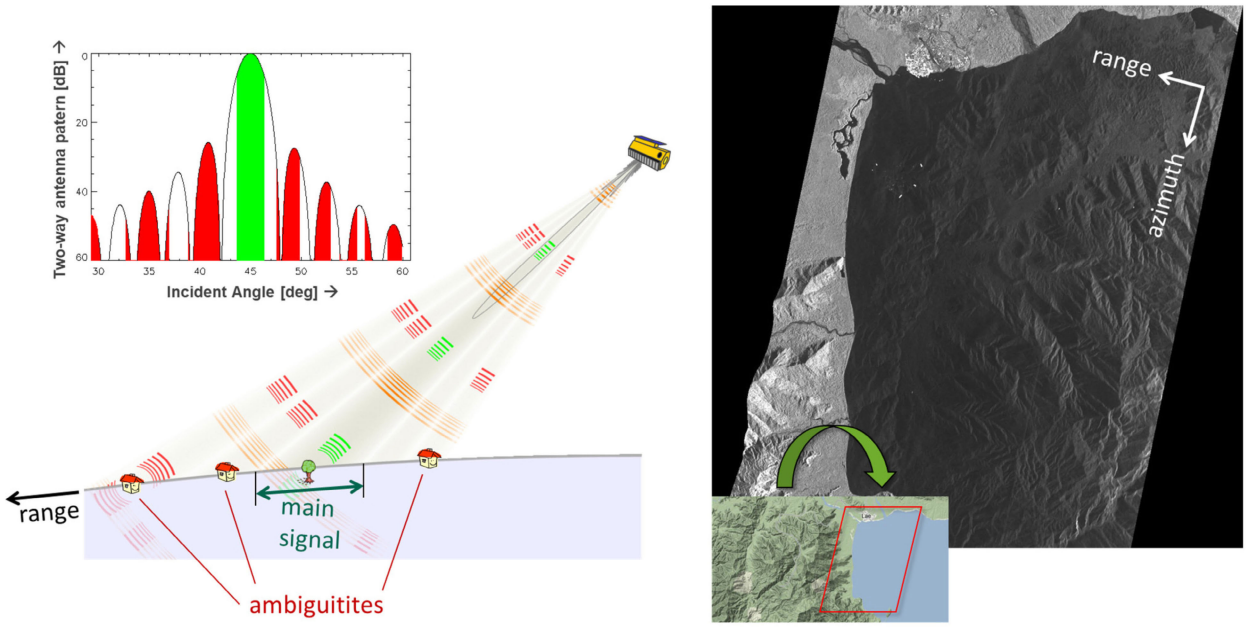

Fig. 5. ***Range ambiguities in SAR systems. Areas outside the desired swath are illuminated through the elevation antenna sidelobes. The echoes from those areas overlay with the desired echoes, thus impairing the interpretability and quality of the final SAR image (transmitted pulses in orange, main echo signal in green, and range ambiguities in red). The image on the right shows an example of range ambiguities in a TerraSAR-X acquisition, acquired over the Solomon Sea near the city of Lae, Papua New Guinea.***

within the main beam, as depicted in the left image of Fig. 5. The echoes of the areas illuminated with the antenna sidelobes are depicted in red, whereas the desired echoes are depicted in green. The right image of Fig. 5 shows a TerraSAR-X scene over a coastal area strongly affected by range ambiguities. The PRF of the radar was set at a high value to accentuate the range ambiguities in the image. Similar to Fig. 3, the range ambiguities can be clearly observed over low backscattering areas, water in this case. For the given example, the range ambiguities come from the area further away from the imaged swath. Depending on the timing of the radar, range ambiguities may also come from the near-range region between the imaged swath and nadir.

Range ambiguities also play a prominent role in the design of SAR systems, as the range elevation beamwidth needs to match the maximum swath imposed by the PRF [see (5)]. A too small antenna size in elevation means a wider swath illumination, but will result in stronger range ambiguities. On the other hand, reducing the PRF such that the swath matches a wider elevation beamwidth will result in higher azimuth ambiguities, unless the azimuth antenna size is increased, leading to a degradation in azimuth resolution.

Fig. 4 summarizes what has been presented so far: the tradeoff between high azimuth resolution and swath coverage. A SAR system design can be either optimized for a high azimuth resolution or a wide swath, but it is not possible to achieve high azimuth resolution and a wide swath simultaneously with conventional systems. For the sake of the example, the table in the middle of Fig. 4 presents the maximum achievable swath width as a function of the desired azimuth resolution, which has been derived using the equations presented above. The SAR design constraint can be overcome by means of advanced SAR system concepts, as expounded in Section III-A.

A further metric to be considered when designing a SAR system is the noise-equivalent sigma zero (NESZ), which is defined as the backscattering coefficient for which the signal-to-noise ratio (SNR) is equal to 0 dB [4]. Therefore, it provides the sensitivity of a SAR system to detect signals with a low backscattering coefficient, analogous to the radar range equation in conventional radars. A proper NESZ (below -20 dB in conventional SAR systems) adds several tradeoffs in the design of a SAR system, including antenna size, distance to the scene (platform altitude), transmitted signal bandwidth, and transmitted average power.

Summarizing, spatial resolution, swath coverage, range and azimuth ambiguities, and NESZ drive the design of a SAR system. The interrelation of these metrics has been the focus of research for decades, fostering the development of SAR technology and concepts.

B. SAR Imaging Modes

A SAR system can be operated in different acquisition modes. Section II-A has focused on the stripmap mode [see Fig. 6(a)], where the radar illuminates continuously the same strip on the ground. However, additional modes

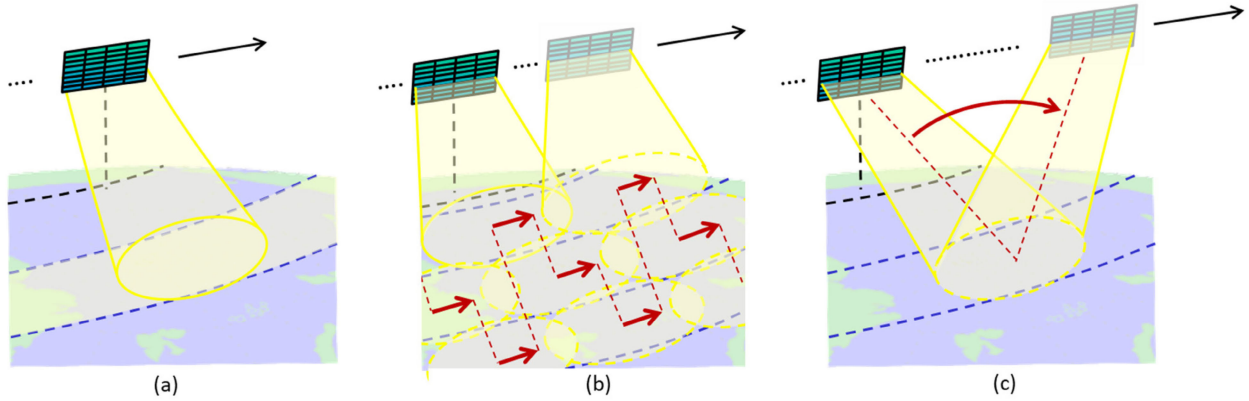

Fig. 6. *SAR imaging modes: (a) stripmap, (b) ScanSAR, and (c) spotlight. Stripmap and ScanSAR imaging modes provide continuous imaging with a typical swath width of 30–80 km and a spatial resolution of 3–7 m (stripmap), and 100–450 km with 15–40 m (ScanSAR). Spotlight mode provides very high resolution (down to 25 × 25 cm) of focused areas (e.g., 10 × 10 km) and cannot achieve continuous imaging due to the antenna steering on the imaged area, which can be accomplished electronically with a phased array antenna or by rotating the satellite.*

have been developed in order to trade spatial resolution with swath coverage. Burst acquisition modes, like ScanSAR [33] and terrain observation by progressive scans (TOPS) [34], achieve a larger swath coverage at the expense of azimuth resolution. As depicted in Fig. 6(b), the larger swath coverage is achieved by periodically switching between elevation beams in order to illuminate adjacent subswaths, such that the synthetic aperture time is shared among them. This reduction of the observation time of the targets results in a decreased azimuth bandwidth and, consequently, worse azimuth resolution. The duration during which a subswath is illuminated is commonly called a burst, and the full scanning cycle time is designed such that each target on ground is illuminated at least by one burst during the desired observation time. Table 1(a) shows the resolution and coverage of a burst mode based on the Sentinel-1 satellite, which is mainly operating in TOPS mode over land. Sentinel-1 covers a swath of 250 km with a spatial resolution of 20 m in azimuth or, alternatively, 400 km, with a 40-m azimuth resolution. Please note that Table 1 shows typical values that may vary depending on the user requirements for a specific SAR mission. In general, full-fledged SAR systems have requirements for global coverage, while NewSpace SAR for small areas with very high spatial resolution.

The alternative to achieve an azimuth resolution better than in the stripmap mode is by means of the spotlight mode [27]. As indicated in Fig. 6(c), through the steering of the spacecraft platform or antenna beam, in this mode, the radar illuminates continuously the same area, or spot, on ground, thus increasing in this way the synthetic aperture time. Consequently, the azimuth spatial resolution will be improved at the expense of azimuth coverage. Note that the system PRF is still the same as in the stripmap mode since the radar must be operated such that the instantaneous bandwidth is properly sampled. As opposed to the stripmap mode, however, the SAR processor needs to handle the fact that the target bandwidth is larger than the PRF by using additional processing steps [27], [28], [35], [36].

Table 1(b) presents the main system specifications of a future high-resolution wide-swath (HRWS) SAR system, which overcomes the resolution-swath tradeoff by means of DBF techniques, as described in Section III. An HRWS system increases the acquired information in terms of

Table 1 User Requirements for Spaceborne SAR Systems. (a) Current full-fledged SAR systems. (b) Future full-fledged SAR systems. (c) NewSpace SAR constellations

State of the Art (e.g., Sentinel-1C)	Imaging Mode (**single/dual pol.**)		
	Extra wide-swath	Wide-swath	Stripmap
Resolution	**40 m**	**20 m**	**5 m**
Swath Width	**400 km**	**250 km**	**80 km**
Orbit Duty Cycle	**25 minutes per orbit**		

(a)

Future Requirements (e.g., Sentinel-1NG)	Imaging Mode (**quad pol.**)		
	Mode X	Mode Y	Mode Z
Resolution	**5 m**	**2 m**	**1 m**
Swath Width	**400 km**	**200 km**	**100 km**
Orbit Duty Cycle	**> 50 minutes per orbit**		

(b)

Requirements (e.g., Capella Space)	Imaging Mode (**single pol.**)	
	Stripmap	Spotlight
Resolution	**2 m**	**25 cm**
Swath Width	**25 km**	**10 km**
Orbit Duty Cycle	**Few minutes**	

(c)

resolution cells (i.e., swath width and spatial resolution) by an order of magnitude when compared to the system specifications of Table 1(a) and (c).

Table 1(c) presents the main specifications for NewSpace SAR systems. They are characterized by a small area coverage and a very high spatial resolution when operated in the spotlight mode. As expounded later in detail in Section IV, NewSpace SAR systems are characterized by being cheap and light when compared to the systems presented in Table 1(a) and (b). This fact allows for a cost-effective deployment, allowing the operation of constellations with a reduced revisit time.

Fig. 7 provides an overview of SAR satellites launched since the year 2000 as well as SAR satellites under development with planned launch dates in the next ca. eight years. Leading nations in the development of SAR satellites include Canada, China, ESA (consisting of 23 member states and 4 associate members), Germany, India, Italy, Japan, Russia, South Korea, the United Kingdom, and the United States. Several other nations have recently entered this development, including Argentina, Indonesia, Finland, Singapore, and Spain. The most commonly used frequency bands are L, C, and X bands, but also P band (e.g., Biomass) and S band (NovaSAR and NISAR). While only three SAR satellites (ERS-2, ENVISAT/ASAR, and Radarsat-1) were operational in mid-2000, today more than 70 SAR satellites are in orbit and operational. More than the half of these operational satellites are NewSpace SAR systems, which will be described in Section IV. All but two of the SAR satellites shown in Fig. 7 are in LEO, i.e., between ca. 500- and 800-km altitude above the Earth. In December 2024, China launched the first very LEO (VLEO) satellite, Haishao-1, with an X-band SAR payload at an altitude of 350 km. China also launched the first geosynchronous SAR satellite, Ludi Tance-4, in August 2023. It has an inclined geosynchronous orbit at 36,000 km describing a figure of eight centered at 89.5° east longitude and extending to ±16° latitude, providing medium spatial resolution with a revisit time of one day. Further studies have been conducted on medium Earth orbit (MEO) SAR satellites, which can provide global coverage in two–three days at medium spatial resolution from an orbit of 6000 km [37]. The development of SAR satellites for global coverage and short revisit times will continue to focus on LEO systems due to the rapid cost reductions achieved in recent years through the emergence of satellite constellations. In Fig. 7, the abbreviations "dual, quad, and compact pol" stand for the polarimetric imaging modes of the radar instrument, whereby H and V mean horizontally and vertically polarized waves. Dual pol represents the imaging mode with two polarizations, typically co- and cross-polarized (e.g., HH and HV or VV and VH, the first letter being the transmitted polarization and the second letter being the receive polarization), quad pol means HH, VV, HV, and VH, and compact pol means transmitting a single circular polarization and receiving both linear polarizations. Polarization diversity provides additional information on the scatterers' geometry and electrical properties [10], [38], [39].

III. ADVANCED SAR INSTRUMENT ARCHITECTURES

While the performance of spaceborne radar systems has significantly evolved over the past decades, the imaging capabilities of conventional SAR instruments are still rather limited. Fig. 8 shows a performance comparison of state-of-the-art SAR systems in terms of spatial resolution and coverage. As a representative example, Sentinel-1 can acquire SAR images with an azimuth resolution of 20 m and a swath width of 250 km in its standard interferometric wide-swath (IW) mode by employing the TOPS data acquisition technique described in Section II. In stripmap mode, the resolution can be improved to 5 m, but only at the cost of narrowing the swath down to 80 km. These examples demonstrate that current SAR satellite missions are not capable of achieving high spatial resolution and wide swath coverage at the same time, an issue that can be traced back to the "fundamental limitation" [48] of the conventional SAR technology as detailed in Section II.

The last decades have seen intense research activities toward new SAR system designs and architectures that employ not only one, but multiple digital channels in their receiver chain [49], [50], [51], [52], [53], [54], [55], [56], [57], [58], [59], [60]. This move toward SAR instrument architectures equipped with DBF capabilities marks a paradigm shift. It allows, among other benefits, to overcome the aforementioned fundamental limitation of conventional SAR systems in terms of resolution and swath width. In fact, these new systems are well-suited to improve the imaging performance of future SAR systems by one or even two orders of magnitude if expressed in terms of acquired resolution cells per second. The extended mapping capabilities of this new generation of multichannel SAR systems go hand in hand with the increasing demands of the scientific user community for frequent, global-scale, and high-resolution SAR image products and provide a suitable means to cost-efficiently serve future Earth observation applications.

A. DBF Synthetic Aperture Radar

The virtue of DBF SAR is that it extends the dimensionality of the trade space [61], allowing for more flexibility in the selection of the instrument, operation, and antenna parameters [57], [58], [62], [63], [64]. The basic principle and added value of DBF is seen in the antenna array and front-end technology: conventional SAR systems are implemented using phased array antennas where transmit/receive modules (TRMs) equipped with analog phase shifters (or true time-delay lines) and attenuators are used to set the antenna array excitation coefficients. As illustrated in Fig. 9, left, the RF signals received by the individual antenna elements are then linearly superimposed in a combiner network, before demodulating,

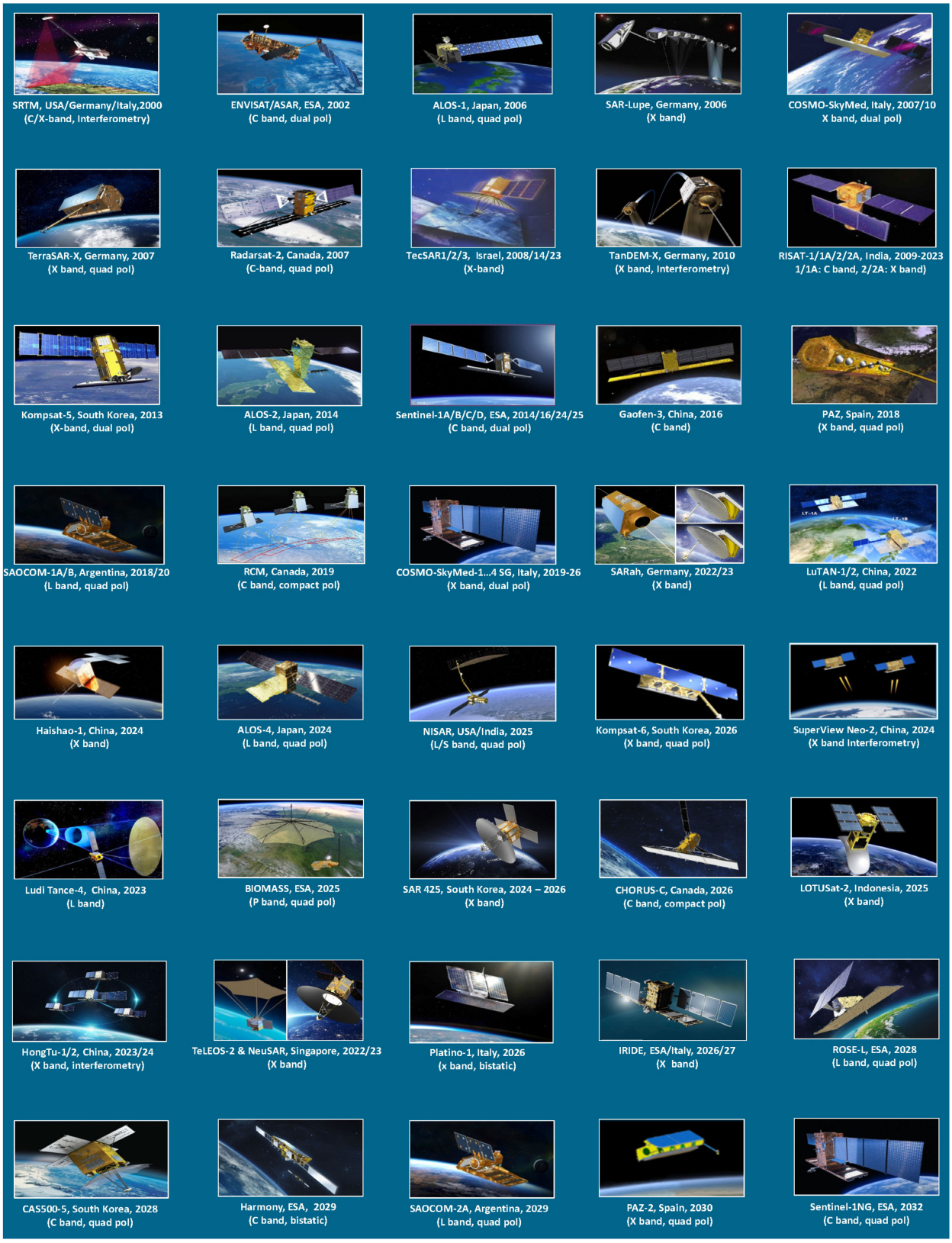

Fig. 7. ***Overview of past, current, and planned full-fledged spaceborne SAR systems (2000 onward, sources: https://www.eoportal.org/; https://space.oscar.wmo.int/; and https://space.skyrocket.de). The dates indicate the launch year of the satellite or satellite series. NewSpace SAR systems are shown in Fig. 13 and described in Section IV.***

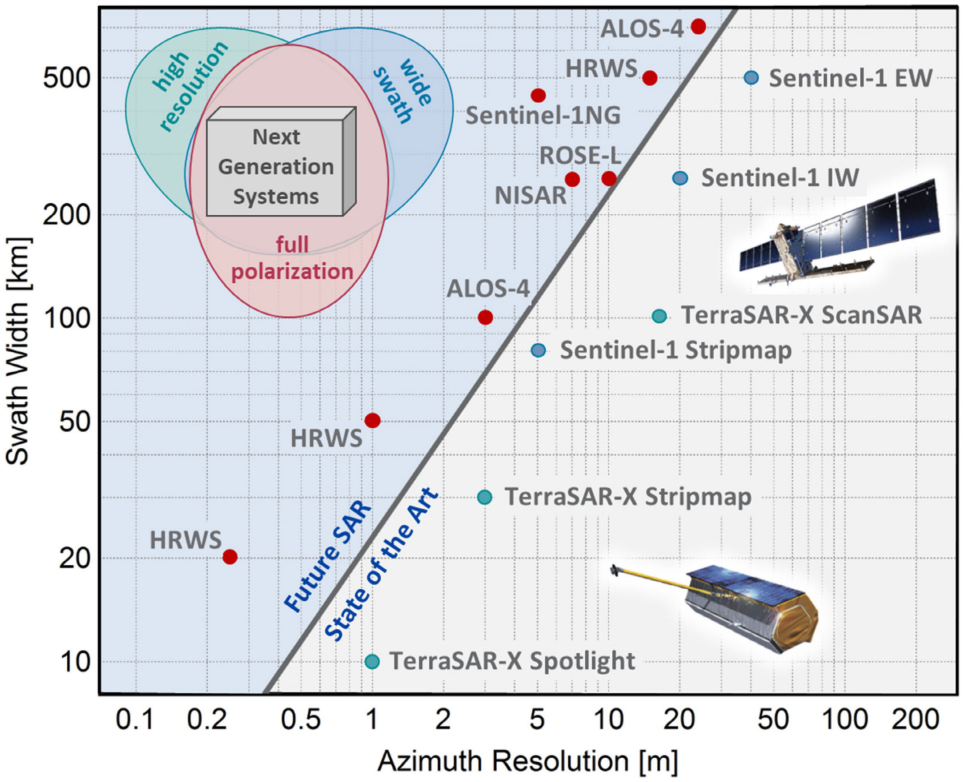

Fig. 8. *Imaging performance of current and next-generation spaceborne SAR systems. The oblique line divides the lower swath-to-resolution ratios achievable by conventional SAR systems (bottom-right gray area) from those obtainable by advanced SAR instruments employing DBF (top-left blue area). The cyan circles show the performance of TerraSAR-X (DLR) and Sentinel-1 (ESA) representing "conventional" SAR missions, while the performance values indicated by the red circles represent in-orbit (ALOS-4, [40], NISAR (NASA/ISRO), [41], [42]) and planned SAR missions (Sentinel-1 NG (ESA) [43], ROSE-L (ESA) [44], [45], and HRWS [46], [47]) with DBF capabilities given in its various implementations. The top-left corner indicates the performance of SAR systems with the full utilization of multichannel DBF capabilities.*

digitizing, and downlinking the single radar signal to the ground for SAR processing. The beamforming, affecting the shape and pointing of the array's radiation pattern, is controlled by the amplitude and phase of the array coefficients, and only a single beam can be formed at each instant of time. This is in contrast to the case of a DBF instrument (see Fig. 9, right), where the radar signals received by the antenna elements are individually sampled and quantized such that the beamforming is implemented in the digital domain. As the sampled data from each antenna element are available in memory, different beamforming coefficients can be applied to the same set of received radar data, which is equivalent to forming multiple simultaneous (digital) antenna beams. The capability to acquire radar data with multiple channels and to form antenna beams in a highly flexible manner is at the core of the tremendous performance improvements that can be achieved by SAR systems with DBF in terms of resolution, swath width, sensitivity, and ambiguity suppression. The performance improvements mentioned above are related to two intrinsic DBF techniques that are applied in the antenna elevation and azimuth directions and are detailed in Section III-B. Further opportunities for improvement arise from the manifold ways to operate a DBF SAR instrument. For example, DBF can be combined with the burst-mode operation introduced in Section II to map an ultrawide swath with high azimuth resolution. Another example is innovative SAR modes that employ multiple elevation beams in combination with a continuous variation of the PRF. These advanced SAR modes are introduced in Section III-C. Additional opportunities arise from the use of DBF techniques not only for the reception of the radar echoes, but also for the transmission of sophisticated radar pulses with a nonseparable space–time structure. The discussion of such multiple-input multiple-output (MIMO)-SAR systems is beyond the scope of this article, and the reader may refer to [57], [63], [65], [66], and [67] for further information.

In terms of the DBF instrument hardware, the digital interface is moved closer to the antenna. Consequently, the complexity of the RF hardware may be reduced, while the demand for the onboard digital processing capabilities grows [42], [55], [68], [86]. A SAR with DBF can be realized with either a planar direct radiating antenna or a parabolic reflector that is illuminated by a digital feed array, as illustrated in Fig. 10 [75], [76], [86]. Although

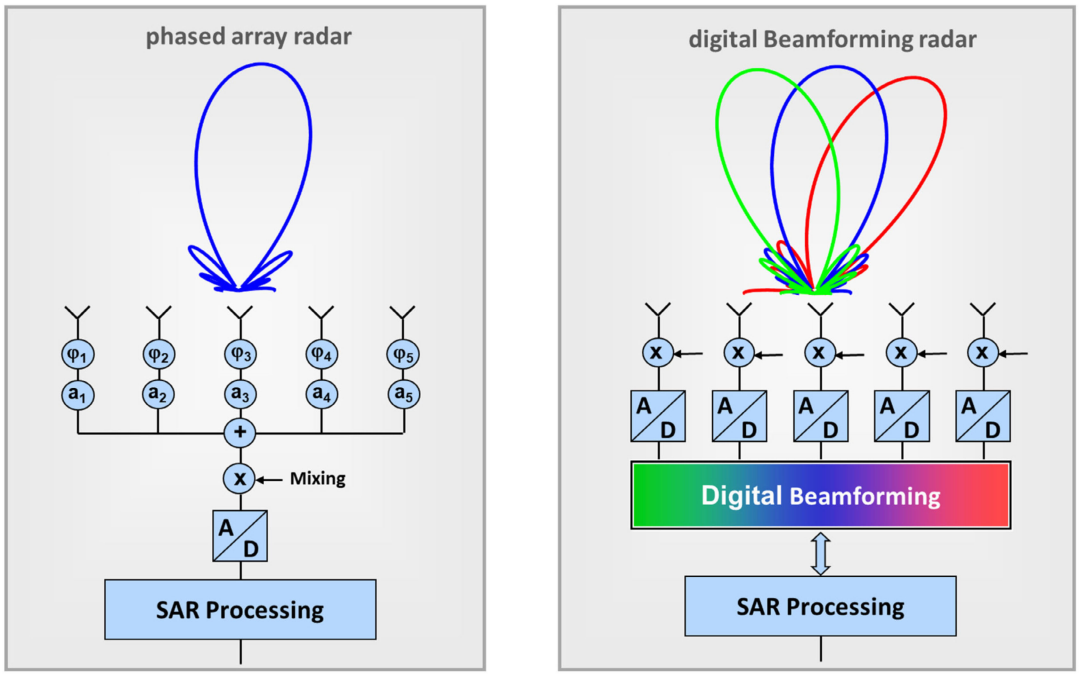

Fig. 9. *Schematic architecture of analog beamforming commonly implemented using TRMs (left) and DBF applied on the sampled data streams (right). Here, front-end components such as amplifiers, filters, and downconverters are not shown.*

the basic DBF architecture from the right-hand side of Fig. 9 is representative for both antenna types, the technique behind the beam pointing is rather different. While the beam direction for a planar direct-radiating antenna is determined by the gradient of the linear phase excitation along the antenna elements, the beam direction of a reflector depends on the position of the activated feed element. This affects not only the way how DBF is performed during the reception of the radar echo, but it also has intricate consequences for the illumination of a wide swath. While a wide beam is generated with a reflector antenna by activating all antenna feeds, beam spoiling is

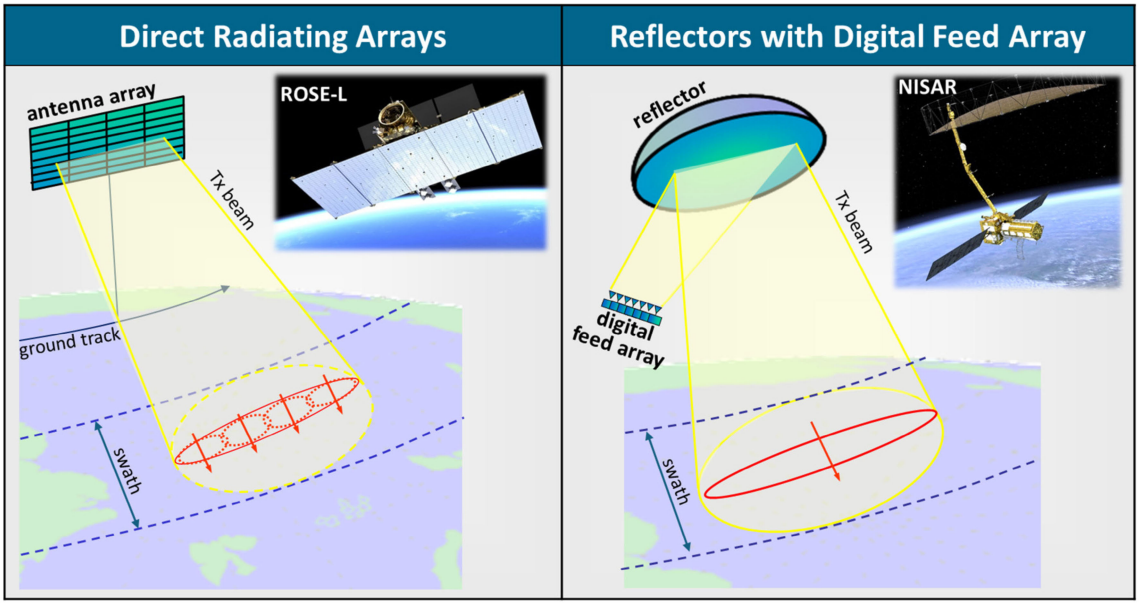

Fig. 10. *DBF implemented for a direct radiating planar-antenna SAR system such as for ESA's planned ROSE-L mission [44], [45] (left) and reflector antenna with digital feed array as implemented for the NISAR mission by NASA/ISRO [41], [42].*

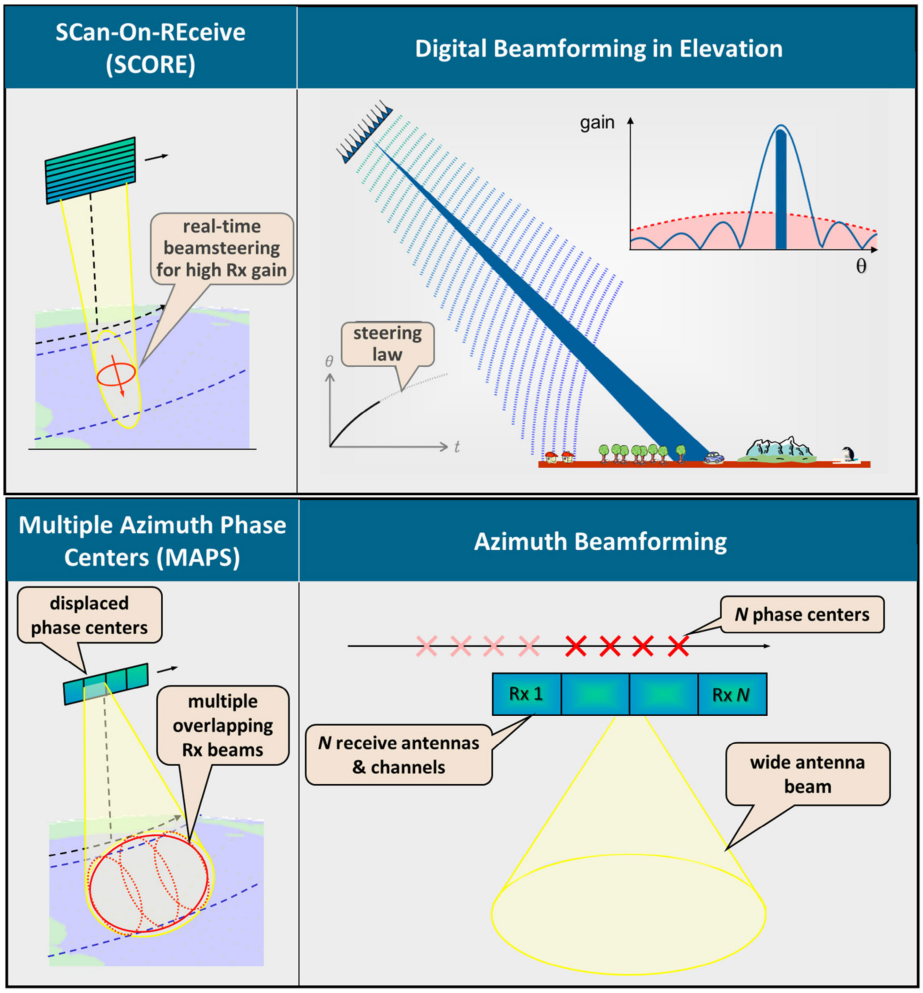

Fig. 11. ***Intrinsic DBF imaging techniques for SAR as implemented for a planar antenna: SCORE concept (top) and displaced phase center antenna (bottom).***

utilized, e.g., by phase-only tapering, to make use of all TRMs in a large direct-radiating array. Sections III-B–III-D will show several examples of how DBF can be used with both antenna types to improve the performance and mapping capabilities of future SAR systems.

B. Intrinsic DBF Techniques

1) SCan-On-REceive: In [70], a basic approach for analog beam steering using variable phase shifters is proposed. This approach allows the receive beam of a planar antenna to move across the swath in accordance with the position of the radar echo. Two decades later, this concept finds further elaboration and justification [53], [54], [71]. The concept presented in [71] extends the idea to reflector antennas, while [53] and [54] introduced DBF techniques in conjunction with a real-time digital beam steering in elevation for the first time.

The SCan-On-REceive (SCORE) technique (see Fig. 11, top) utilizes multiple elevation channels to generate a receive beam that follows the SAR signal echo as it traverses the ground. In this way, SCORE allows the receiving antenna to be enlarged in the elevation dimension without losing full swath coverage. The associated increase in antenna gain improves the SNR, and the narrow receive beam helps to suppress range ambiguities. Note that the transmit antenna beam must remain wide to illuminate the complete imaged swath. This can be achieved by using either a separate narrow antenna for the transmission of the radar signal or by using an appropriate phase tapering of a combined transmit/receive antenna. As the amount of recorded data tremendously increases due to the simultaneous reception with multiple elevation channels, the SCORE technique must be implemented onboard in real time. This requires not only fast digital signal processing, which is usually carried out in a field-programmable gate array (FPGA), but also mutual calibration among the elevation channels on board the satellite. The beamforming implemented through SCORE combines the data streams of the elevation channels into a single output data stream without loss of information and may, thus, be understood as a lossless data compression. In terms of the trade space, SCORE decouples the imaged swath

width from the receiving antenna height, i.e., increasing the antenna height will not reduce the swath width as with conventional SAR systems.

One particularity of enlarging the antenna height with SCORE is that the angular extent of the pulse area contributing to the radar echo at any instant of time (known as the pulse extent [72]) may become comparable to the antenna beamwidth. This effect—which can be associated with a loss of information—should be compensated, e.g., through the implementation of a dispersive SCORE [53], [54], [73], [74], as it would otherwise lead to a degraded range resolution and radiometric bias [72].

In summary, SCORE is well-suited to enhance the SNR and suppresses range ambiguities. However, it does not allow for a significant expansion of the imaged swath width, as it will be described in the following.

2) Multiple-Aperture Processing Scheme (MAPS): The rationale behind the use of multiple azimuth channels can be understood by recalling from Section II that azimuth ambiguities arise from an insufficient sampling of the Doppler spectrum. A wide Doppler spectrum is, however, a prerequisite to achieve a high azimuth resolution. In a traditional SAR, an improved azimuth resolution implies, therefore, also an increase of the PRF, which inevitably results in a reduction of the swath width due to the increase of range ambiguities. This fundamental design dilemma of the conventional SAR systems can be overcome by using multiple phase center sampling in combination with a dedicated multiple-aperture processing scheme (MAPS) in azimuth. To explain the basic idea behind this solution, we distinguish in the following between planar and reflector SAR systems [75], [76].

For the planar system, all antenna elements cover the same wide angular segment, thus "seeing" identical Doppler spectra as shown in the bottom left of Fig. 11. Consequently, azimuth ambiguities can be suppressed by augmenting the spatial sampling of the Doppler spectrum, which is accomplished by adding digital channels in the flight direction [50], [51], [53], [56], [58]. Let us consider a single transmit event and compare the sampling of the radar echo by a conventional single-channel SAR with that of an advanced SAR with N azimuth channels. As shown in the bottom right of Fig. 11, the latter provides N times the number of samples along the synthetic aperture for each transmitted pulse. Therefore, multiple azimuth channels with antenna phase centers mutually displaced from each other in the flight direction allow a broader Doppler spectrum to be sampled without rising azimuth ambiguities. This, in turn, enables a finer azimuth resolution, while the PRF, determining the swath width, is inversely proportional to the total antenna length and independent of the azimuth resolution.

A reflector system with multiple azimuth channels uses a set of feeds that are mutually displaced in the along-track direction [73], [74], [75], [76]. In contrast to the planar case, each element "sees" a different angular segment of the reflected radar echoes. As each segment is associated with a narrow portion of the Doppler spectrum, it can be sampled at a low Nyquist rate, which is inversely proportional to the size of the reflector. By combining the narrow spectra of all azimuth channels, a wide Doppler bandwidth and, thus, a fine azimuth resolution can be recovered without increasing the PRF or reducing the swath width.

Both the direct radiating and the reflector antenna implementations of the multiple azimuth channel technique result in a higher data volume. As the increased data rate is also associated with a higher information content in the form of a finer azimuth resolution, it is necessary to separately store the data streams from different azimuth channels on board and then downlink them to the ground without further onboard processing. This has the advantage that both an accurate calibration and a sophisticated multichannel data processing can be carried out on the ground [60], [77], [78], [79], [80]. Unlike SCORE, where an on-ground calibration would require an undesired increase in the downlink data rate, here, the multiple azimuth channel data are necessary for on-ground processing.

In summary, multiple azimuth channels are well-suited to enhance the azimuth resolution without any need to increase the PRF and narrow the swath width. The improved resolution is, however, also associated with an increase in the data volume that has to be transferred to the ground.

C. Advanced SAR Modes With DBF

The intrinsic DBF techniques introduced in the previous section can be combined and extended to obtain advanced modes for high-performance SAR imaging, as illustrated by the representative examples in Fig. 12 and discussed in this section.

Clearly, the SCORE and the MAPS techniques can be combined, as shown in the top left of Fig. 12 [51], [53], [54], [73], [82]. Here, the large width (height) of the receive antenna yields a good sensitivity, while multiple azimuth channels are utilized to obtain a fine azimuth resolution. The azimuth resolution could, in this example, be improved almost arbitrarily by increasing the number of receive channels and shortening the length of the transmit antenna and the receive subapertures. The swath width is, however, still limited by the total length of the receiving antenna, as it is necessary to transmit a radar pulse every instant of time when the receive antenna has moved half of its total length. This becomes clear from the bottom right of Fig. 11, where one can see that a lower PRF would, otherwise, result in gaps along the synthetic aperture. A very long antenna would, therefore, be required to map an ultrawide swath (35–40 m for a 400-km swath [83]).

As for a conventional SAR, the need for such a long antenna can be avoided by employing the ScanSAR or TOPS mode introduced in Section II. In burst-mode operation, the total Doppler spectrum is shared among all bursts,

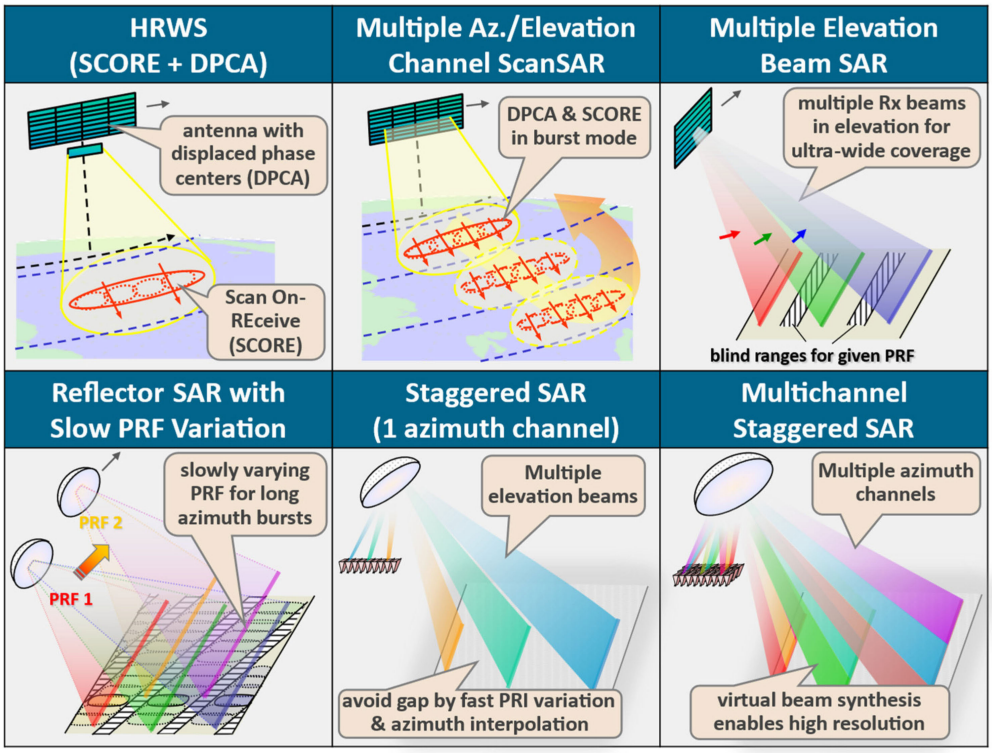

Fig. 12. ***SAR imaging modes and system architectures for HRWS SAR imaging (adapted from [81]). HRWS SAR with real-time DBF in elevation and multiple Rx channels in azimuth [53], high-resolution ScanSAR with multiple azimuth channels [84], planar multiswath stripmap SARs with multiple elevation beams [83], multiple elevation beam SARs with slow PRF variation [89], staggered SAR with fast PRI variation [91], and high-resolution staggered SAR with multiple azimuth channels [76] (from top left to bottom right). All system concepts and modes can, in principle, be implemented by either planar direct radiating array antennas or by reflector antennas with digital feed arrays.***

which limits the available Doppler bandwidth for each target and results in a degraded azimuth resolution. The loss in Doppler bandwidth can, however, be compensated by utilizing MAPS, as illustrated in the top center of Fig. 12 for the case of a direct radiating planar array that is divided into multiple subapertures. Here, the use of multiple subapertures in azimuth avoids the resolution loss from burst-mode operation, while SCORE in elevation enhances the sensitivity, thereby compensating the loss in transmit gain that results from illuminating a wider Doppler spectrum [84], [85]. This multichannel ScanSAR mode will be used in the upcoming ESA Copernicus L-band SAR mission ROSE-L [44], [45], and it is also foreseen for the next generation of Sentinel-1 SAR satellites [43].

Another promising option to extend the SAR imaging performance is to illuminate an ultrawide swath with a high PRF and utilize the system's beamforming capability in elevation to map not only one but multiple subswaths. This can be accomplished by employing multiple (digital) SCORE beams at the same time, each recording the radar echoes from a different subswath, as illustrated in the top right of Fig. 12. The imaged swath consists, therefore, of several subswaths, and the total swath width may be extended by adding more SCORE beams at the cost of an increased data rate. Such a multiple-elevation-beam SCORE system can be implemented with either a direct radiating array or a reflector antenna that is illuminated by a feed array [49], [57], [82], [83]. The latter case is also denoted as SweepSAR [86] and forms the basis for the NISAR mission from NASA/ISRO [41], [42].

Although the basic idea behind this technique is straightforward and appealing by making additional use of the available elevation channels, it is also associated with a number of challenges. First, it poses higher requirements on range ambiguity suppression as several swaths are illuminated at the same time and their radar echoes must be mutually separated during the signal reception by using sufficiently narrow elevation beams with low sidelobes [73], [76], [87]. A second and similar challenge may be nadir echoes, which can also be suppressed by the elevation beamforming and, if necessary, by employing additional nadir suppression techniques [88]. Third, the reception of the radar echoes is interrupted when the instrument is transmitting, as the receiver (hardware) of single-platform SAR systems is blinded during high pulse power transmission times. This introduces blind ranges (for example, two blind ranges for a 350-km swath) that separate the subswaths and prevent the SAR from imaging a wide contiguous swath.

To eliminate the gaps between the subswaths, burst-mode operation, such as ScanSAR or TOPS, can again be employed to image a wide continuous swath. Here, two bursts are in principle sufficient to eliminate all gaps and to map an ultrawide swath [83]. An inherent peculiarity of such a multiple elevation beam ScanSAR mode is the constant burst length for all subswaths. As a result, the azimuth resolution will vary with range. The performance of the two-burst multiple-elevation-beam ScanSAR mode can be improved by using additional PRF values or even a continuous variation of the PRF, as illustrated in the bottom left of Fig. 12, where the blind ranges migrate slowly through the wide swath [83]. By choosing an appropriate saw-tooth sequence of periodically increasing or decreasing PRIs, one can optimize the available burst lengths for all ranges that are longer than those for the twin PRF case [89]. The SAR focusing of the individual bursts requires a (simple and straightforward) interpolation of the azimuth raw data to a uniform sampling interval. A drawback of these multiple elevation beam burst modes is that a wider portion of the Doppler spectrum is illuminated than required for a given azimuth resolution. While this over-illumination can be used to acquire additional azimuth looks, it also results in a waste of signal energy, thereby increasing the power demands of the satellite.

An alternative to the slow PRF variation is a change of the PRI such that the gap positions of two successive transmit pulses never impact the same range [83], [90]. The "missing" samples can, then, be recovered using suitable azimuth interpolation techniques, thereby avoiding the periodic interruption of the synthetic aperture in the burst modes and enabling an efficient stripmap-like operation over the full swath width as illustrated in bottom center of Fig. 12. This SAR mode is suitable for both reflector and planar-antenna systems, and it has been analyzed in a number of publications where it is denoted as staggered SAR [64], [91], [92], [93], [94]. While it has been demonstrated that azimuth interpolation based on the signal statistics can efficiently be used to recover the samples lost during the transmit events, this necessitates also an oversampling (by a factor between 1.5 and 2) in the azimuth domain, i.e., an increase of the PRF, leading to a higher susceptibility to range ambiguities and a nonnegligible increase of the data volume. The former can be mitigated by increasing the antenna height and utilizing more advanced elevation beamforming techniques. The latter requires either increased onboard storage and downlink capacity, or data reduction through appropriate azimuth filtering and resampling to a uniform grid [93], which must be performed onboard and requires a substantial increase in (digital) processing complexity and resources. Staggered SAR has been considered as a promising solution for the reflector-based wide-swath SAR mission NISAR [41], [42] as well as for the mission proposal Tandem-L [95], [96].

While staggered SAR is suited to map an ultrawide swath with a stripmap-like resolution, one can improve the azimuth resolution by adding multiple azimuth channels, as shown in the bottom right of Fig. 12 for the case of a reflector-based system. Here, additional feeds in the along-track direction acquire multiple squinted data streams, which cover different portions of a widened Doppler spectrum. To combine the data streams from the multiple feed elements into a set of uniform samples along the synthetic aperture, a technique known as virtual beam synthesis has been developed. Here, azimuth beamforming is applied to samples from successive radar echos to effectively position the azimuth samples on a regular grid [76], [97].

D. Summary DBF Imaging Performance

In summary, multichannel SAR and DBF can significantly enhance SAR performance by potentially redirecting the effort from the analog RF domain to the digital processing domain. Specifically, SAR systems equipped with DBF capabilities can be utilized to achieve a high resolution and wide swath, while improving the sensitivity and ambiguity suppression. Table 2 gives an overview of different DBF techniques. The first two intrinsic DBF techniques (SCORE and MAPS) are shown in Fig. 11 for a planar-antenna implementation; other advanced DBF techniques are depicted in Fig. 12 for a planar antenna (top row) and digital feed with reflector antenna (bottom row). Principally, all the DBF techniques may be realized with a planar direct radiating antenna or a reflector antenna in combination with a digital feed array (see Sections III-A and III-B). The proper choice depends on many factors and the application; a reflector antenna may be favorable at lower frequencies in terms of antenna area and weight or for mapping SAR missions, whereas a planar-antenna DBF SAR offers advantages for highly flexible user-driven missions with agile beam pointing. While DBF techniques allow for an improved SAR system performance and imaging capacity, they are associated with an increased radar system complexity and new challenges, such as multichannel receive hardware, calibration accuracy between channels, onboard real-time data processing for beamforming or data reduction, and sophisticated SAR image processing algorithms for the payload ground segment.

Fig. 8 shows the comparison of the performance of conventional SAR systems with that of the next-generation DBF systems in terms of imaged swath width and azimuth resolution. For example, Sentinel-1 NG will achieve a spatial resolution of 25 m^2 and a swath width of 400 km, while keeping the radiometric sensitivity at a similar level as the first generation [43], thus enabling new applications to be implemented without reducing the imaging quality. This represents an improvement in imaging performance (in terms of acquired resolution cells per second) by one to two orders of magnitude.

IV. NewSpace SAR

Over the last decade, NewSpace SAR has driven the development of high-resolution SAR constellations. Cost-effective, lightweight systems based on NewSpace concepts

Table 2 Comparison of Different Digital Beamforming (DBF) Techniques

DBF SAR Technique	Advantage	Disadvantage
SCORE (Scan-On-REceive)	Increased antenna gain and SNR; improved suppression of range ambiguities	Swath width limited by timing; increased antenna height; requires on-board real-time [digital] beamforming and channel calibration; pulse extension loss may lead to radiometric bias (can be avoided by dispersive beamforming)
MAPS (Multiple Azimuth Phase Center Sampling)	Improved azimuth resolution (unambiguous swath width and PRF remain constant for fixed antenna length); azimuth beamforming and channel calibration performed on ground	Adding digital channels causes a higher instrument complexity; increase of downlink data rate (due to finer resolution); timing limitations due to operation close to uniform PRF, otherwise possible worsening of SNR
SCORE & MAPS (with stripmap mode)	Combined advantages of SCORE and MAPS; stripmap imaging mode	Combined disadvantages of SCORE and MAPS; antenna length increases significantly if a wide swath is required
SCORE & MAPS with Burst Mode (ScanSAR)	Improved azimuth resolution compared to conventional single channel ScanSAR mode; total antenna size remains constant compared to the stripmap realization; well suited for direct radiating antennas	Wide swath requires large number of bursts; in combination with a high azimuth resolution, this leads to a large squint angle variation and increased susceptibility to scalloping
SCORE with Multiple Elevation Beams	Ultra-wide swath by simultaneous imaging of multiple sub-swaths in stripmap mode; increased antenna gain and SNR; azimuth resolution may be further improved by MAPS	Blind ranges (typically 2 to 4) occur between the sub-swaths; increase of antenna height and/or number of elevation channels to suppress range ambiguities; increase of downlink data rate (due to wider swath)
Two-Burst ScanSAR with Multiple Elevation Beam SCORE	Ultra-wide swath imaging with only two ScanSAR bursts; improved azimuth resolution (if compared to conventional ScanSAR); increased antenna gain and SNR	Worsened azimuth resolution due to sharing of Doppler spectrum (if compared to stripmap); increased antenna height and/or number of elevation channels to suppress range ambiguities; low transmit power illumination efficiency in elevation
Slow PRF Variation with Multiple Elevation Beam SCORE	Ultra-wide swath imaging with improved performance and resolution if compared to Two-Burst ScanSAR mode; elimination of blind ranges through slow PRF variation and long bursts	Worsened azimuth resolution if compared to stripmap mode; lower SNR due to unused parts of Doppler spectrum (which may, however, provide additional looks)
Staggered SAR	Ultra-wide swath imaging with multiple elevation beams; elimination of blind ranges by fast PRI variation; fine stripmap-like azimuth resolution (full Doppler spectrum available); avoids inefficiencies of burst mode operation	Requires azimuth oversampling by a factor of 1.5 to 2; oversampling causes higher data rate or requires additional on-board processing for azimuth sample interpolation and data reduction; increase of antenna height and/or number of elevation channels to suppress range ambiguities
Staggered SAR with Multiple Azimuth Channels	As for Staggered SAR, but azimuth resolution is improved by multiple azimuth channels; such a DBF-SAR technique is considered the most powerful for full-fledged SAR systems with requirements for ultra-wide swath (e.g. 400 km) and very high azimuth resolution (e.g., 1-2 m)	Additional complexity required for azimuth virtual beam synthesis (to be performed on-ground); on-board accurate calibration of azimuth channels required; increased downlink data rate

are continuously deployed to image small areas at very short revisit times, complementing complex SAR missions with global coverage. NewSpace SAR constellations are characterized by an ultracompact SAR system design aiming at a spatial resolution of a few decimeters over small regions of interest [98]. NewSpace SAR marked a turning point for spaceborne SAR in that NewSpace SAR companies are fueled by venture capital and focused on commercial applications, whereas full-fledged SAR systems have so far been mainly funded by space and/or defense agencies. This section discusses the user requirements, commercial applications, and enabling technologies of NewSpace SAR missions and provides some notable examples of systems in operation.

A. User Requirements and Commercial Applications

The term NewSpace refers to the pursuit of nongovernmental market objectives, primarily driven by market

Fig. 13. ***Examples of NewSpace SAR systems with the respective number of satellites launched as well as planned launches (in brackets) as of October 15, 2025 [101], [102]. ICEYE, Capella, and Umbra are leading the commercialization of NewSpace SAR imagery, followed by iQPS and Synspective. Typical weights of NewSpace SAR satellites are in the range of 85–250 kg, much less than full-fledged SAR systems, weighing approximately 1–2.5 ton, due to their much greater imaging capacity and coverage.***

forces, which carry out activities in an entrepreneurial way. This is, therefore, in contrast to pursuing objectives set by governments, with boundaries defined by sociopolitical forces, tending to act risk-averse, mainly based on public funding, and producing sustainable innovations and improving capabilities [99]. Numerous commercial players have entered the NewSpace business, raising funds to launch constellations of small satellites for communication and remote sensing, including SAR. The total amount of funds raised for NewSpace SAR satellites has already exceeded one billion dollars and is expected to increase further, with a significant impact on the Earth observation data market.

The first NewSpace SAR system was the X1 demonstrator of the Finnish company ICEYE, launched at the beginning of 2018 by an ISRO PSLV-C40 rocket and delivering its first image three days later [100]. After ICEYE, which has meanwhile launched over 40 SAR microsatellites, further NewSpace SAR companies, including Capella Space (USA), Synspective (Japan), Spacety (China), iQPS (Japan), Umbra (USA), and PIESAT (China), also have SAR satellites in orbit. In the timeframe 2018–2024, a total of approximately 95 commercial small SAR satellites were launched [101], [102]. Although most NewSpace companies do not disclose information on the functionality of their satellites in orbit, a rough estimate is that about half of them are currently operational. Fig. 13 displays artist impressions of leading NewSpace SAR systems.

A main feature of NewSpace SAR missions is their ability to access the same location on Earth daily and even subdaily. These very short access times of few hours are achieved through a large constellation of satellites and different strategies.

ICEYE, for example, initially placed all satellites of its constellation in sun-synchronous orbits, which were not evenly distributed, leading to an average time to access a location at the equator of 12 h. At higher and lower latitudes, the rates are more frequent. The ground track repeat cycles varied between 1 and 22 days. Each orbital plane was phased around the Earth with a different local time of ascending node, allowing the overall constellation to observe a location at different times of the day. This has an advantage over dawn-dusk orbits, where the local time of acquisition is always around sunrise or sunset. Moreover, each satellite could slowly adjust its orbits throughout its operational lifetime by raising or lowering the altitude of the spacecraft in its orbital plane. This changes the orbital period, which, in turn, changes the repeat period of the ground track. As the fleet grew, it was gradually being tuned to coherent ground tracks that repeat daily. This offers new possibilities for combining identical data collections of the same area while maintaining fast access times [103]. Very recently, ICEYE has launched some satellites in mid-inclination orbits to provide more imaging opportunities at middle latitudes [104].

Umbra also flies its satellites in sun-synchronous orbits as the first four satellites of Synspective (the fifth satellite is in an orbit with a lower inclination). The Capella satellites instead operate in different orbits with average inclinations of 45° (525-km altitude), 53° (575-km altitude), and a sun-synchronous orbit with 97° (525-km altitude). The orbits have an orbital period of about 97 min, which, with

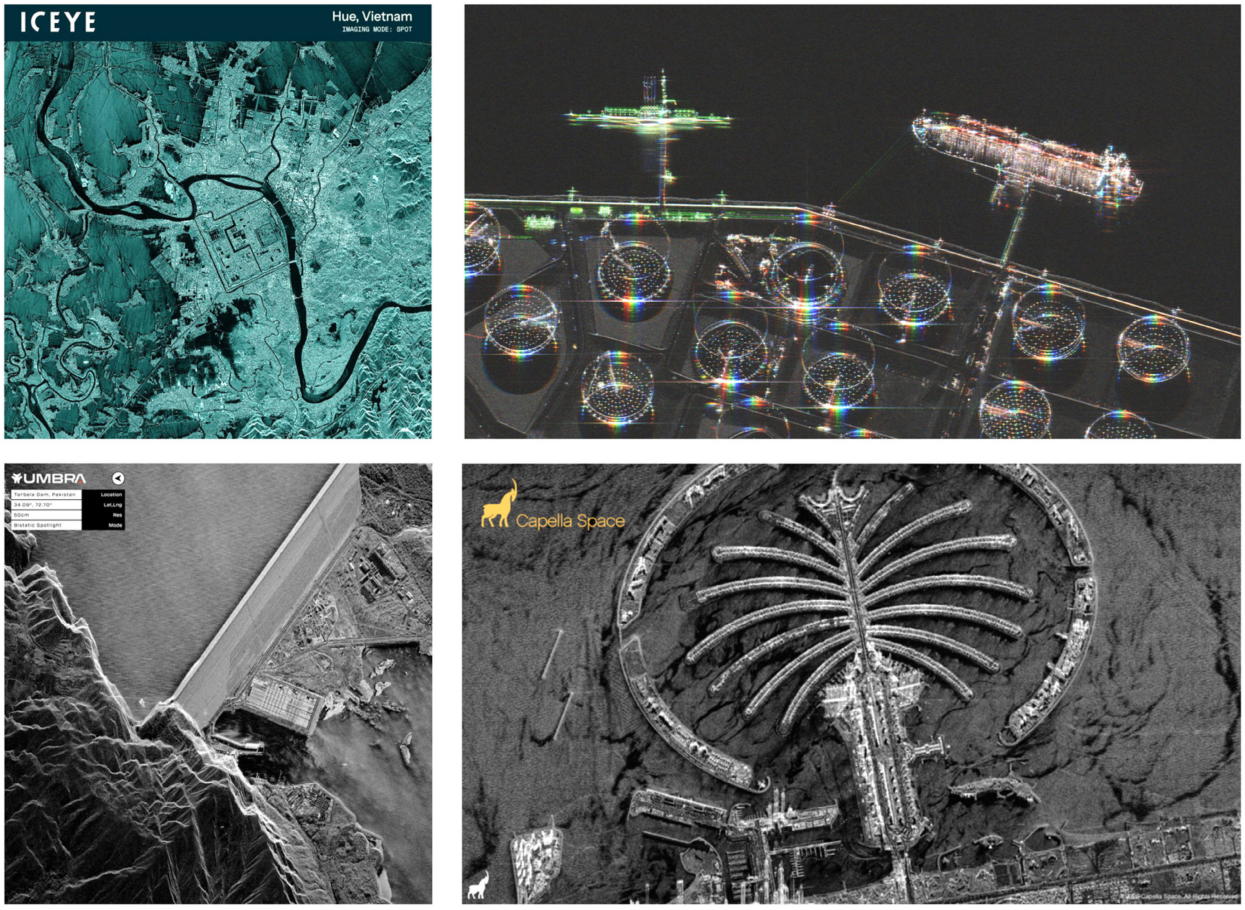

Fig. 14. *Examples of SAR images acquired by NewSpace SAR systems: ICEYE, Hue Vietnam (top left), ICEYE Dwell mode, Rotterdam, The Netherlands (top right), Umbra, bistatic SAR image of Tarbela Dam, Pakistan (bottom left), and Capella, Palm Islands, Dubai, United Arab Emirates (bottom right). Image credits: ICEYE, Umbra Space, and Capella Space.*

eight satellites, allows for an access time of 2–5 h [105]. The satellites in the Capella constellation are currently not in repeat track orbits, meaning that they do not always pass over the same place on the Earth in a consistent cycle. Recurring tasks that require consistent geometries can, therefore, be captured less frequently.

While the very limited orbital duty cycle does not make those missions suitable for continuous global coverage as traditional satellites, such as Sentinel-1, NewSpace SAR systems aim at mapping small areas at the highest possible resolution. A peculiarity of many of these systems is the Dwell imaging mode, a very long data collection in staring spotlight mode, where the satellite stares at the same point for several tens of seconds [106]—please refer also to Section II. The technique is facilitated by the smaller mass and antenna size of the satellites and allows achieving azimuth resolutions in the subdecimeter range, resulting in product resolution down to 25 cm (after multilooking by a factor of 5 over 5 km $\times$ 5 km spots, as it is the case of ICEYE's Dwell Precise imaging mode. ICEYE offers a variety of products with different tradeoffs between product resolution, the number of looks, and imaged area, among which the spot extended area mode with a product resolution of 1 m (after multilooking by a factor of 2 over 15 km $\times$ 15 km spots is claimed to map the largest area for that specific ground resolution [106]. High-resolution products of comparable quality are also offered by Capella and Umbra [108], [109]. Some examples of high-resolution images are displayed in Fig. 14. Using phased-array antenna technology, ICEYE also offers ScanSAR imaging of wide swaths of up to 100 or 200 km with moderate spatial resolution of 15 and 27 m, respectively, a unique feature for NewSpace SAR systems so far [107]. The cost of high-resolution images is in the order of a few hundreds of dollars, corresponding to 15 \$/km^2 [101]. Some companies, such as ICEYE and Umbra, also have the option of selling ready-made satellites, as an alternative to SAR data.

Several additional products derived from SAR imagery, such as colorized subaperture images and video products obtained from the Dwell collection, are often offered together with the standard images. As the distribution of SAR images in civilian applications is limited to 25-cm resolution, data are decomposed into different azimuth

subapertures, and the resulting images are combined through color-coded schemes so that the target scattering behavior can be better visualized. Further, subaperture processing during the long Dwell illumination time allows the generation of video animations, showing the displacement of slow-moving targets such as ships or ocean waves in the SAR image.

The applications served by NewSpace companies spread over a wide range. Downstream services are mainly based on defense and security, but also include hazard and crisis monitoring, illegal vessel detection, oil spill tracking, and scientific applications. The detection and classification of the services offered by Capella, for instance. Millimeter-scale change detection, also referred to as coherent change detection, related to, e.g., the assessment of damages caused by natural catastrophes, and the monitoring of infrastructure integrity, is enabled by the daily coherent ground track repeat option of ICEYE, which ensures that each image of the stack is acquired in the same imaging geometry. The latter application also relies on a large amount of archived data, which can be used alongside new imagery. Among the peculiar applications offered by Synspective is the use of spaceborne SAR data to observe wind speed and wave height to optimize offshore wind power [110].

Two of the NewSpace companies in Fig. 13, namely, PIESAT and China Siwei, have already launched and commissioned their NewSpace SAR satellites, HongTu-1 and SuperView Neo-2, respectively, that fly in close formation and enable bi-/multistatic SAR, opening up an even broader spectrum of applications, as described in Section V. Capella and Umbra have exploited some specific opportunities to carry out experimental bistatic acquisitions using two distinct satellites and large bistatic angles [111].

B. Enabling Technologies

NewSpace SAR solutions show a high degree of innovation in technology, processes, and mission operations. The total mass of NewSpace SAR satellites is comprised between 85 and 250 kg, which makes some of the satellites even belong to the category of microsatellites (mass below 100 kg). As a term of comparison, the TerraSAR-X satellite weights 1230 kg and Sentinel-1 2300 kg.

The most commonly employed frequency is X band (with Spacety using C band instead). X band is attractive for multiple reasons: first, it is very popular with potential users, as it is already widely used. Second, the same antenna size offers greater gain at a higher center frequency and can be used up to higher angles of incidence before range ambiguities constrain performance. Third, ITU regulations now allow a bandwidth of up to 1.2 GHz (9.2–10.4 GHz) for the Earth observation, allowing ITU-compliant SAR systems to provide the aforementioned very high spatial resolutions [112]. Both planar and reflector-based antennas are used. In particular, Capella Space's instrument with its 3.2-m reflector also allows for a significant reduction of the peak power (600 W) compared to traditional satellites at the cost of reduced coverage.

The satellites are one–two orders of magnitude cheaper than full-fledged SAR systems, with the cost of a single NewSpace SAR satellite rarely exceeding $15 million. A cost comparison of NASA instruments and commercial NewSpace SAR instruments by payload mass is discussed in [101] and shows that the latter are far less expensive even for satellites in the same mass class (e.g., a factor of ten for 200-kg spacecraft), albeit satellite lifetime and radar performance parameters (e.g., transmit power, duty cycle, and area coverage) are not explicitly accounted for in the analysis. Due to the use of commercial off-the-shelf (COTS) components as well as limited system redundancy and platform resources (e.g., fuel and battery capacity), a reduced lifetime is achieved, typically less than three years, which explains why about half of the NewSpace SAR satellites launched are no longer operational.

The aforementioned cost reduction is achieved through a number of factors, starting from the massive use of COTS components. This also allows accessing the very latest capabilities in the field, as space-qualified components, while very reliable, usually do not provide the latest features. As an example, Capella employs an NVIDIA GPU on all its satellites, which allows for real-time onboard processing of their SAR imagery. Moreover, most COTS components have been miniaturized, thus leading to a smaller size and mass. Of course, there is an additional risk in not using parts that have been specially built and qualified for operation in space because the space environment is hostile and unpredictable, but the idea is to launch a constellation of satellites and tolerate the fact that if one spacecraft fails, there are always the others to step in. Components are sourced to balance reliability with cost. NewSpace SAR satellites are usually designed to work for a few years, and the constellations are planned to be replenished at regular intervals with more advanced spacecraft. This allows NewSpace SAR companies to keep improving capabilities in space at the pace with advancements in technology.

Another important factor is power management. Full-fledged SAR satellites image for long periods per orbit cycle and must, therefore, be designed to gather and store the solar energy required to operate the radar instrument and dissipate the heat generated in the process, which has a corresponding impact on size and weight. For LEO satellites, one orbit cycle corresponds to approximately 97 min. In order to achieve global coverage of the land masses, full-fledged SAR systems operate 20–40 min/orbit cycle. NewSpace SAR systems, on the other hand, operate on short duty cycles, with each satellite imaging for only a few minutes or less per orbit cycle, so these power issues are much easier to overcome, and it is possible to cope with potential downlink constraints. And again, with many satellites, it is possible to cover large areas or image the same location more often.

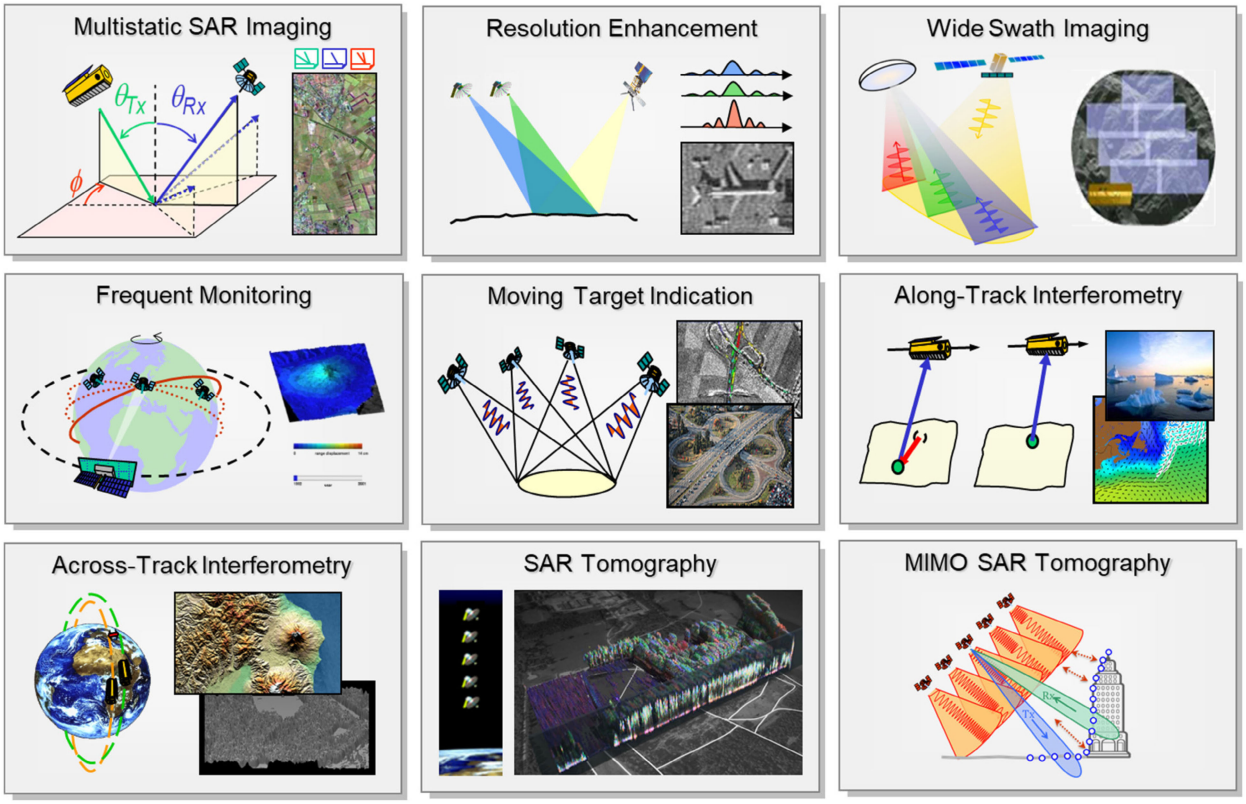

Fig. 15. ***Opportunities from bistatic and multistatic SARs. Multistatic SAR imaging: increasing image information by observation angle diversity [121], [122], [123], [124]; resolution enhancement: increasing Doppler and/or signal bandwidth by angle diversity [132]; wide-swath imaging: continuous illumination of a large area with a bistatic receiver using multiple beams [83]; frequent monitoring: GEO or MEO transmitter with several LEO receive-only small satellites [120]; moving target indication: space–time adaptive processing (STAP) with multiple transmitters and receivers [143]; along-track interferometry: different azimuth phase centers to estimate the velocity of slowly moving targets [163]; across-track interferometry: two or more satellites with across-track separation to estimate the ground topography [140]; SAR tomography: estimation of the vertical profile of volume scatterers [139]; and MIMO-SAR tomography: estimation of different scattering mechanisms (e.g., single- and double-bounce scattering) in tomographic imaging [173] (from top left to bottom right).***

NewSpace SAR satellites exploit electric propulsion for orbit maintenance, collision avoidance, and deorbiting at the end of their lifetime. With the next generation of NewSpace SAR satellites being developed, accurate orbit control becomes possible so that the necessary precision for interferometric applications is achieved.

Gallium nitride (GaN) components with high radiating power are used for highly efficient solid-state amplifiers at X band. This technology has started to become available in the last decade, offering hundreds of watts per amplifier with high efficiency and thus lower thermal dissipation.

A fundamental aspect of the design of NewSpace SAR systems is that the image quality specifications in terms of NESZ, ambiguity, and calibration are not as demanding as full-fledged SAR systems. The specification on the NESZ rarely exceeds −20 dB, and the total range and azimuth ambiguity-to-signal ratio is often accepted to be worse than −17 dB, leading to a relaxation of the requirements on the average transmit power and antenna size. The degradation of the image quality due to ambiguities and nadir echoes is mitigated through the use of waveform diversity and multifocus postprocessing and novel techniques to suppress azimuth ambiguities by detecting them and filtering them out [88], [113], [114], [115]. In this context, newly proposed "ambiguous" SAR modes could also play an important role by providing "noisy" high-resolution SAR images over ultrawide swaths of several hundred kilometers without the need for DBF or multiple apertures. Such modes are effective for dedicated applications such as ship detection [116], [117].

Besides commercial players, a number of satellites designed according to the NewSpace SAR principles discussed above have also been developed by national space and defense agencies. Notable examples are Italian constellation IRIDE, Vietnamese LOTUSat 1, South Korean CAS500-5, and Singaporean NeuSAR and TeLEOS, where the latter is characterized by a near-equatorial orbit with an inclination of 10° [118].

V. BISTATIC, MULTISTATIC, AND DISTRIBUTED SAR

The simultaneous observation of a scene using multiple platforms not only provides additional opportunities for increasing the information content in the multidimensional data space, but also paves the way for a new class of information products that help the scientific community

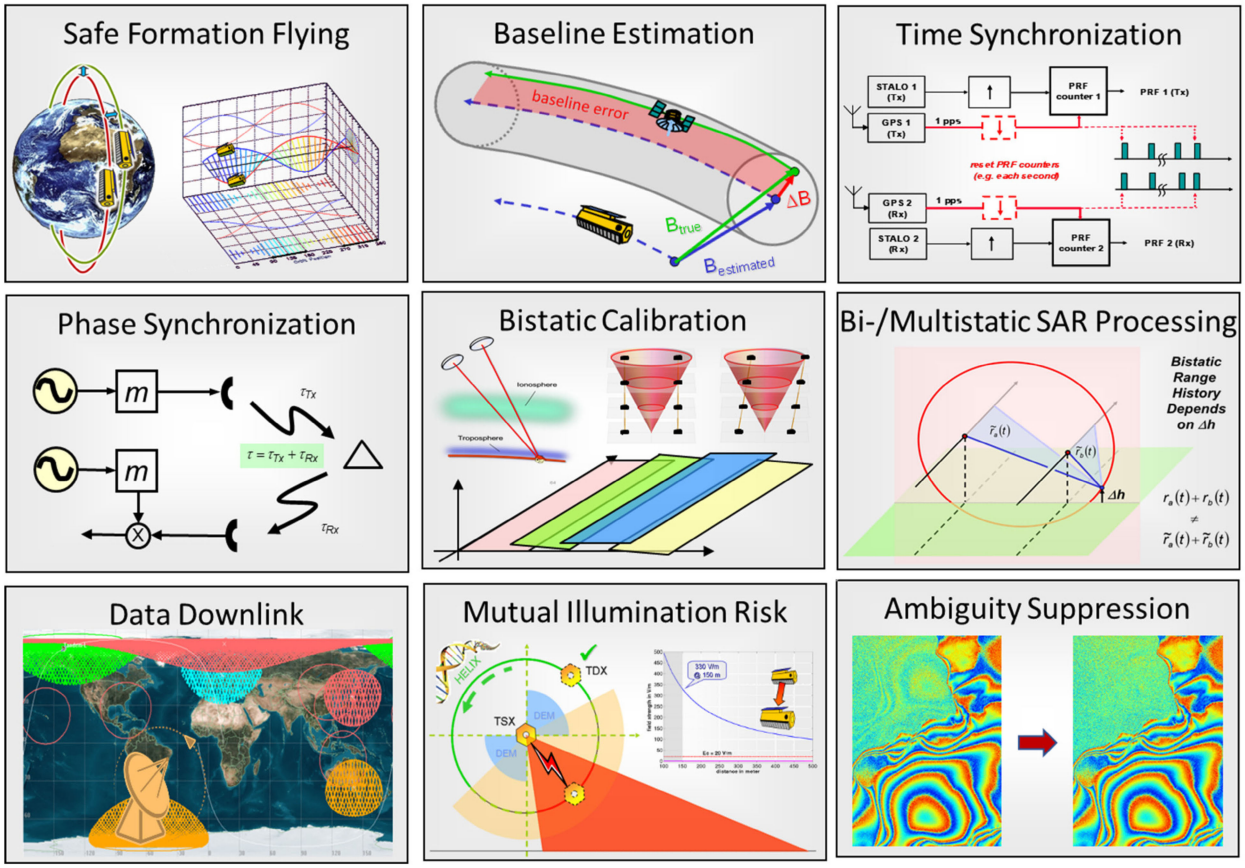

Fig. 16. *Challenges of bistatic and multistatic SARs. Safe formation flying to avoid collision between the satellites [144]; baseline estimation to allow accurate estimation of the topography [146]; time synchronization to ensure the same PRF reference for each radar [141], [142]; phase synchronization between the transmitter and receiver radar systems [142], [150], [151], [153]; bistatic calibration to remove residual amplitude and phase errors of the bistatic system [142]; bi-/multistatic SAR processing to address the specific requirements of the bistatic geometry [122], [123], [124], [159]; data downlink of a large amount of data using several ground stations over the Earth [141]; consideration of the mutual illumination risk to prevent the transmitter to damage the receiver [141], [142]; and suppression of coherent ambiguities in the interferogram [160], [161], [162] (from top left to bottom right).*

to understand and quantify dynamic processes within the Earth system [119]. This section addresses the opportunities and challenges of bistatic SAR systems, in which the transmitting and receiving antennas are located on different platforms, and multistatic SAR systems, in which the echo of the transmitted signal is simultaneously collected by receiving antennas located on multiple platforms. Graphical overviews of the opportunities and the challenges of bistatic and multistatic SAR are provided in Figs. 15 and 16, respectively. The main distributed SAR techniques enabled by multistatic configurations are introduced, along with an overview of the concepts and missions for their implementation.

A. Opportunities From Bistatic and Multistatic SAR Systems

Bistatic and multistatic radars have been an area of interest for military applications to achieve improved target detection capabilities, as the electromagnetic scattering process of natural and man-made targets is highly sensitive to the incidence, scattering, and out-of-plane angles [119]. In the case of spaceborne and airborne SAR, several experiments have shown that monostatic and bistatic SAR images of the same scene might significantly differ, even for a small bistatic angle of only a few degrees [121], [122], [123], [124], [125]. Therefore, the availability of bistatic images considerably expands the observation space, far beyond multiangle monostatic images [119]. The analysis of bistatic radar cross sections, less influenced by retroreflector effects, mostly improves the detection and recognition of targets, and the comparison between monostatic and bistatic backscatter coefficients can aid the segmentation and classification in SAR images [126]. Additional opportunities arise from forward scattering geometries, where suitable bistatic configurations could help to observe a desired scattering mechanism, e.g., in a forest scenario [127]. The combination of bistatic imaging with polarimetry has further potentialities, as cross-polarized responses

could exceed the co-polarized ones for some out-of-plane angles, and require particular attention in the interpretation and use of the data [128].

A multistatic system, where receiving antennas on multiple platforms record the echoes received from a common illuminated area, can be regarded as a distributed sparse aperture and exploited for resolution enhancement. If the platforms are arranged as a train in the along-track direction, the received signals can be combined in a coherent way following the same principle as the multiple azimuth aperture system described in Section III [129]. As a minimum safety distance between the satellites of the formation must be maintained, the range lines collected from the same transmitted pulse by the multiple receiving antennas will not be blocks of consecutive range lines in azimuth, as is typically the case in a multiple aperture system, but will be interleaved with range lines collected from different transmitted pulses. The exploitation of multiple platforms for alternated or simultaneous transmission allows reducing the required average power per platform [130], [131]. An alternative configuration for resolution enhancement is represented by platforms arranged in the across-track direction, where the coherent combination of multiple SAR images acquired from slightly different incident angles can improve the range resolution, as proposed in [132], and thus even overcome the bandwidth limitations for spaceborne SAR sensors imposed by international frequency regulations. A formation of platforms arranged in across track can also be exploited for increasing the mapped swath width through multiplatform suppression of the range ambiguities and avoid the problem of blind ranges in systems with multiple elevation beams (see also Section III) [133].

The platforms that host the transmitting and receiving antennas can be located very far away and on different orbit types. In particular, concepts based on a geostationary illuminator and multiple passive receivers in LEO allow for a sensible reduction of the revisit times and can be exploited for frequent monitoring. The analyses in [120] show that it is possible to achieve an NESZ of less than -19 dB in the vicinity of the receiver nadir for a transmit power aperture product of 10^5 W·m^2 and a 6-m^2 receive antenna at X band. The adaptation of this concept to geosynchronous, medium Earth, or highly elliptical, high-inclination (e.g., Molniya) orbits would overcome the latitude limitation imposed by a geostationary illuminator.

Besides increasing the imaging capability in terms of mapped swath or achieved resolution, multistatic SAR systems open the door to a completely new class of imagery-based information products, which include velocity maps, accurate digital elevation models (DEMs) through SAR interferometry (InSAR), and high-resolution tomograms that unveil the 3-D structure of vegetation, ice, and dry soil [8], [135], [136], [137], [138], [139]. DEMs and tomograms can also be obtained from repeat-pass monostatic SAR images, but multistatic SAR systems enable much better quality, thanks to the absence of temporal decorrelation and the reduced impact of atmospheric effects, as demonstrated by the TanDEM-X mission, which generated a DEM of the Earth with unparalleled quality and resolution [20], [140]. The availability of multiple baselines in a single pass massively boosts the DEM performance and extends the fields of application to the monitoring of fast-changing phenomena, such as the assessment of permafrost degradation through the difference of DEMs acquired at short time intervals, from which accurate estimates of volume changes over time can be derived. Finally, the exploitation of multiple transmitting antennas can help infer useful information on the scattering mechanisms through the concept of MIMO SAR tomography [173].

B. Challenges of Bistatic and Multistatic SAR

Many multistatic configurations foresee close satellite formations and, therefore, require a careful orbit selection together with reliable collision avoidance strategies. An effective solution, employed in the context of the TanDEM-X mission and that can be generalized to the case of more than two spacecraft, is the Helix formation that combines an out-of-plane (horizontal) orbital displacement by different ascending nodes with a radial (vertical) separation by different eccentricity vectors resulting in a helix-like relative movement of the satellites along the orbit [144]. As an alternative, fixed-baseline formations could be considered (in the case of small baselines), which require implementation of a continuous control, e.g., using low-thrust engines, to avoid oscillation due to the natural dynamics and keep the desired spacecraft separation [145]. In particular, maintaining a fixed baseline in the across-track direction would be beneficial for multibaseline single-pass SAR interferometry for DEM generation and for multiplatform range ambiguity suppression.

The relative spacecraft positions of a multistatic system need to be estimated to a great accuracy, as position errors in the order of a centimeter might lead to notable interferometric phase errors for typical SAR frequencies and especially at short wavelength, e.g., in X band, which would impact the absolute height error of the DEM [120]. In the case of close satellite formations, measurements using differential Global Navigation Satellite System (GNSS) guarantee accuracies of the interferometric baseline vector estimation down to a millimeter after calibration [146].

A major challenge of bistatic and multistatic SAR is the synchronization between the transmitter and receiver [120]. While in monostatic systems, the low-frequency phase errors due to the oscillator's nonidealities cancel out since the same oscillator signal is used for modulation and demodulation, in bistatic and multistatic systems, phase errors not only lead to a defocusing of the SAR image, but also to visible distortions through the observed scene [147]. In particular, a difference in the oscillator frequencies with a consequent linear phase error will determine a shift of the bistatic impulse response, a quadratic phase

error will result in a widening of the mainlobe of the impulse response, and high-frequency components will cause an increased level of sidelobes.

Different solutions have been devised for synchronization of multistatic systems, the most relevant of which are the following [148].

1) Continuous synchronization of the USOs, where two spacecraft continuously transmit and receive their local oscillator signals [149].
2) Mutual exchange of radar pulses via a dedicated synchronization link, where pulses are transmitted either in duplex or alternated mode. The latter option is also used in TanDEM-X, where six horn antennas are used on each satellite to cover all solid angles [150]. A similar approach is also used in Lutan-1, where the loss of imaging echoes is avoided through appropriate timing (noninterrupted synchronization) [151].
3) Exploitation of ground control points in combination with hyper-stable oscillators [152].
4) Alternating transmit mode, where the oscillator phase differences are extracted from the bistatic echoes [153].
5) GNSS-based synchronization, in which the radar payload and the GNSS receiver share the same oscillator, and the phase error is inferred from the GNSS data and the results from the precise orbit determination. This approach is well-suited to systems with multiple receive-only platforms [154].
6) Data-based synchronization, where synchronization is solely achieved through the evaluation of the received bistatic data exploiting the azimuth diversity resulting from multichannel architectures or along-track formations [155].

Other synchronization concepts are also possible, as it has been proposed for MirrorSAR [156], [157], [158]—see also Section V-D.

The focusing of bistatic SAR data requires specific algorithms that precisely accommodate two relevant effects, namely, the azimuth variance and the topography. Time-domain approaches can be used based on subaperture processing, where the images obtained from different subapertures are displayed in coordinate systems capable of incorporating the topographic information [159].

Further effects might arise when multiple SAR images are jointly processed. One example is the coherent effect of azimuth ambiguities in SAR interferometry, observed for the first time in TanDEM-X interferograms, which lead to significant biases in the interferometric phases and modulations of the coherence magnitude with visible artifacts in the resulting DEM [160]. A theoretical model for the coherent effect of ambiguities helps consider it in the design of interferometric SAR systems. Furthermore, strategies have recently been devised to coherently remove azimuth ambiguities through a postprocessing step or to decorrelate them through a slight variation of the PRI [161], [162].

Further challenges include the bistatic operation and commanding, the downlink of the acquired data, the avoidance of mutual illumination, which could harm the electronics of the satellites of the formation, mode compatibility for companion satellites, redundancy, mutual interferences, tropospheric and ionospheric delays, acquisition conflicts, development and launch schedule, as well as cost and programmatic aspects.

C. Multistatic SAR Techniques: From Interferometry to Distributed SAR Concepts

In the following, an overview of the distributed SAR techniques enabled by multistatic systems is provided.

SAR interferometry exploits the coherent interference between two images acquired from slightly different positions, whose connecting segment, whether physical or virtual, is called the baseline. In along-track interferometry, the baseline is aligned with the satellite tracks, and thus, it is possible to acquire two images of the same scene with the same observation geometry and a time lag (in the order of tens of milliseconds) that can be exploited to measure line-of-sight displacements and therefore “instantaneous” radial velocities [163]. This technique was originally developed for ocean surface measurement, but can also be used for moving object detection. Whereas the ocean surface velocity could be in theory estimated from a single baseline, additional baselines allow compensating for the Bragg scattering components due to wind and avoid significant estimation biases [164].

The case where the time lag or temporal baseline between the acquisitions is in the order of several weeks up to years is referred to as differential SAR interferometry. While this technique does not necessarily require multistatic acquisitions, a satellite formation with large squint diversity, given by the large along-track distance between the illuminator and the receivers, allows retrieving of different projections of the deformation and therefore accurate 3-D global deformation measurements of the Earth’s surface [165]. The availability of simultaneous acquisitions allows the retrieval of the North–South deformation with outstanding accuracy, as most of the tropospheric signal is correlated among the lines of sight and, therefore, cancels out for this component. For this reason, the large angular diversity can be further exploited to retrieve not only the deformation, but also the absolute differential tropospheric delay [166].

In across-track interferometry, the baseline is perpendicular to the satellite tracks, and the two viewing angles can be exploited to infer information about the third dimension and form accurate DEMs by exploiting phase measurements [8], [135]. Whereas the two SAR images could be in principle acquired from the same platform, larger baselines lead to a better accuracy of the height estimation and motivate the use of multistatic systems.

Unfortunately, as the baseline increases, the phase variation of the interferogram becomes faster (especially in areas with slopes facing the radar) and, in the presence of noise, might lead to unwrapping errors, i.e., the phase value cannot be associated with the correct 360° phase cycle, a fundamental step to form a DEM. For that, a third image acquired from a point closer to one of the two satellites can help solve this problem at the cost of either an additional acquisition or a third satellite, which can also be a CubeSat with a smaller aperture [167], [168]. In the context of single-pass multibaseline InSAR, if a large chirp bandwidth is available, e.g., 1.2 GHz at X band, radargrammetry can be exploited to aid in phase unwrapping [169].

A recent development for the generation of accurate, high-resolution DEMs of an observed scene in a single pass is based on the exploitation of large sets of noisy and undersampled data acquired by a cluster of receive-only small satellites with small antenna apertures, e.g., using a single transmit-only satellite [170]. The small satellites may be flown in formation in a distributed configuration with different along- and across-track baselines. Small SAR satellites in a distributed formation flight represent a radical paradigm shift from state-of-the-art systems and techniques and take advantage of the fact that a large amount of the information contained in the currently used multidimensional datasets is redundant. The concept of small distributed SAR satellites is a topic of future research and can help reduce the antenna size of the radar satellites and therefore make a single-pass, multibaseline interferometric SAR system more affordable.

The concept of cross-track interferometry can be combined with polarimetry to observe different scattering mechanisms at different polarizations. In particular, SAR systems with low frequencies are sensitive to volumetric backscattering from semitransparent media and allow imaging of internal structures. In this way, polarimetric SAR interferometry, often abbreviated as Pol-InSAR, can provide an initial characterization of the vertical structure of natural and man-made volume scatterers with one or a few baselines [171].

A much larger amount of information about the 3-D structure of vegetation and ice, which would be otherwise very difficult to obtain on a global scale, can be retrieved using SAR tomography [139]. Like in across-track interferometry, observations with baselines orthogonal to the satellite tracks are needed, but in much greater numbers, so that a 2-D virtual aperture can be formed. Multistatic systems allow performing tomographic acquisitions in a single pass or in a much smaller number of passes.

A further new concept to finely resolve the vertical structure of natural media by using a distributed spaceborne SAR system is based on a formation, which operates in MIMO mode by implementing a frequency-division multiplexing (FDM) access scheme, where all satellites transmit simultaneously in different frequency bands and receive the echoes scattered by the Earth's surface in all transmitted bands [172]. As a result, formations of four or five satellites can be deployed to provide the equivalent of 17 and 26 monostatic acquisitions, respectively. Such figures are comparable to the best airborne and ground-based systems available as of today and indicate the concrete possibility to image the vertical structure of natural targets from space at fine resolution [172].

MIMO SAR tomography is a recent idea, which addresses an inherent limitation of conventional radar tomography, namely, the presence of wrong features in the tomographic profiles due to double-bounce scattering [173]. The proposed solution is based on the simultaneous transmission of orthogonal waveforms from multiple antennas and the reception of all backscattered signals by all antennas. From the acquired dataset, different transmit–receive illumination scenarios can be emulated through "a posteriori" beamforming, enabling unambiguous separation of single- and multiple-bounce scattering, where full polarimetry can only help identify which scattering mechanism predominates.

A major limitation of conventional linear SAR methods is the limited view of the measurement of the azimuthal viewing angle. Since the scattering signature depends directly on the observation angle, it is not possible to fully characterize the imaged objects. An alternative to overcome this limitation is the use of wide-angle synthetic apertures, such as holographic SAR tomography, where multiple circular trajectories distributed in height are flown while illuminating the same area on the ground. In this way, a complete 3-D reconstruction with very high resolution over an azimuth angle of 360° can be achieved [174].

Table 3 provides an overview of the main bistatic and multistatic SAR imaging techniques, as well as their measurement capabilities and fields of application. These techniques are based on different interferometric baseline configurations and separations, which can be temporal (in the case of along-track or differential interferometry) or spatial (in the case of across-track interferometry, tomography, and holography).

D. Overview of the Proposed Concepts and Missions

In recent decades, a variety of concepts and missions have been proposed to implement the described multistatic techniques. Without claiming completeness, some of them will be briefly presented.

BISSAT is a concept consisting of flying a passive SAR on board a small satellite that observes the area illuminated by an active SAR, operating on an already existing large platform. The passive satellite is designed without requiring design modification or additional operating complexities to the active illuminator. A key point in the payload design is the development of a light passive antenna of the weight of 31 kg, where azimuth and elevation steering are only considered as an optional feature [175].

Table 3 Bistatic and Multistatic SAR Imaging Techniques for Different Baseline Configurations

Imaging technique	Measurement	Comments
Along-track Interferometry	Ocean current velocity, ice or glacier movement	Time lag from milliseconds to seconds (e.g., Harmony mission). For time lags larger than a few seconds (e.g., for ice movement estimation), repeat-pass interferometry is adopted.
3D Differential SAR Interferometry	Ground deformation in millimetric accuracy	Time lag from hours to decades with repeat-pass interferometry. Multistatic SAR required only for 3D ground deformation vector estimation (e.g., Harmony mission).
Across-Track Interferometry	Surface topography	Typical baselines from a few 100 m to a few 10 km depending on radar frequency and required measurement accuracy.
Polarimetric SAR Interferometry	Height and vertical structure of volume scatterers	Forest height estimation, ice and glacier sublayer imaging using a model-based inversion with one or few baselines.
(Polarimetric) SAR Tomography	3D imaging of volume scatterers and urban environment	3D imaging of forest, ice, glacier and dry soil. Layover- and foreshortening-free 3D imaging of buildings and man-made objects.
(Polarimetric) MIMO SAR Tomography	3D imaging of volume scatterers and urban environment	Same as above, but with improved measurement of different scattering mechanisms (e.g. unambiguous 3D imaging of single- and multiple-bounce scattering).
(Polarimetric) SAR Holography	3D imaging of volume scatterers and urban environment over 360°	3D imaging over 360 degrees of forest, ice, glacier and dry soil. Layover- and foreshortening-free 3D imaging of buildings and man-made objects over 360° observation angle over azimuth.

Cartwheel foresees the acquisition of quasi-simultaneous radar images through a low-cost system based on a set of passive receivers onboard a constellation of microsatellites in a particular orbital configuration. The combination of the images produced by the satellites can improve the final resolution in range and azimuth and systematically produce across-track and along-track interferometric data [178].

TanDEM-X was launched in June 2010 and opened a new era in spaceborne SAR remote sensing. The first formation flying bistatic radar system was built by extending the TerraSAR-X mission by a second, TerraSAR-X-like satellite. The resulting large single-pass SAR interferometer features flexible baseline selection and enables the acquisition of highly accurate interferograms not impacted by temporal decorrelation and atmospheric disturbances. The primary objective of the mission was the generation of a global DEM with unprecedented accuracy, namely, 12-m horizontal resolution and 2-m relative height accuracy (Fig. 17). Furthermore, TanDEM-X has unique capabilities, including along-track interferometry, and new bistatic and multistatic SAR techniques, which support numerous secondary mission objectives. In the last years, the mission has acquired data for a global change layer, showing the height changes relative to the first global DEM dataset, producing a "Change DEM" [20], [181].

SAOCOM-CS is a proposed companion satellite to the Argentinian SAOCOM-1B L-band SAR mission, where the addition of a passively receiving companion flying in formation enables the acquisition of single-pass interferometric and multipass tomographic data [179].

SKADI is a mission proposal for an ESA Earth Explorer Mission Call that aims to assess and quantify dynamic processes in cold environments by measuring the static and dynamic topographies [180]. The SKADI system consists of a cross-platform Ka-band radar interferometer with two spacecraft that fly in a reconfigurable formation and can dynamically adapt to the needs of scientific observation. The use of Ka band minimizes systematic biases and errors in across-track interferometry that would be caused at lower frequencies due to wave penetration into semitransparent media. The expected DEM change products have accuracies in the order of decimeters to centimeters. The short wavelength in Ka band allows a reduction of the size and weight of the antennas and spacecraft and enables the joint launch of two radar satellites with a single medium-sized launch vehicle like Vega C [180]. Although SKADI was not selected for implementation, a Ka-band interferometric SAR mission for cryosphere research remains an important topic [182], [183].

LuTan-1 is the first bistatic spaceborne SAR mission for civil applications in China, which consists of two full-polarimetric L-band SAR satellites operating with flexible flight configurations, which have been successfully launched at the beginning of 2022. In the first phase, the two satellites fly in a formation with a variable baseline,

Fig. 17. ***TanDEM-X mission (left) and DEM of Europe (right). The Copernicus DEM derived from the TanDEM-X data is today a reference of the global Earth's topography [176], [177].***

using bistatic InSAR stripmap mode to acquire digital elevation and terrain models with high accuracy and spatial resolution. In the second phase, the two satellites share the common reference orbit with a 180° orbital phasing difference, decreasing the repeat cycle to four days, so that topographic variations can be measured with millimeter accuracy at a large scale using differential InSAR [184].

Harmony is a concept that has been selected for ESA's Earth Explorer 10 mission and is planned for launch in 2029. The Harmony mission consists of two receive-only companion SAR satellites of Sentinel-1, which serves as illuminator for their bistatic observations. The line-of-sight diversity in combination with repeat-pass SAR interferometry will enable the estimation of small deformations on the Earth's surface, the topography changes on land ice as well as the retrieval of relevant information over oceans (e.g., ocean current velocity) and sea ice (e.g., displacement patterns, fracturing, and deformation) [185].

HRWS is a proposal from German Aerospace Center (DLR) that combines a high-end satellite in X band with low-cost receive-only platforms. The high-end satellite is a stand-alone transmit/receive radar system with high transmit power, DBF capabilities, and multiple azimuth phase centers, which can be flexibly exploited to achieve an azimuth resolution down to 25 cm in spotlight mode or a swath of up to 500 km in ScanSAR mode, as well as to implement the innovative "Theater" acquisition mode, where up to eight spotlight acquisitions in areas of interest can be quasi-simultaneously performed. At a later phase of this study, three small and low-cost receive-only satellites following the MirrorSAR concept were considered to add multistatic interferometric capability and therefore to allow the generation of a DEM with a resolution one order of magnitude better than TanDEM-X [186]. A similar concept is currently being considered for Korean satellite KOMPSAT-8.

MirrorSAR is a multistatic, fractionated mission concept based on a transmit-only spacecraft and several receive-only satellites, where the latter essentially act as mirrors (space transponders) that route the radar signal scattered from the ground to the transmitter [156], [157]. The complexity of the small satellites is reduced by one order of magnitude, while the main satellite may act only as a transmitter. As sketched in the right panel of Fig. 18, the relayed radar signals are then coherently demodulated and combined in the transmitter, which is also responsible for the downlink of the data to the ground. A synchronization signal can, furthermore, be sent from the transmit satellite to the receive satellites, where it is received by a dedicated antenna and superimposed on the radar echo. The overlaid signals are jointly shifted in frequency using a coherent mixer and then radiated back to the transmitter. The superimposed synchronization signal and radar echo are then separated on the ground. The independent up conversion of the receive satellite and down conversion of the transmit satellite introduce phase errors, which are, however, the same for both the synchronization signal and the radar echo. As a result, after separating the synchronization signal from the radar echoes, an evaluation of the synchronization signal allows for the estimation and subsequently correction of these phase errors on the radar echo. The synchronization signal will be then removed from the imaging data through filtering [158].

PLATiNO-1 is the first mission of a wider program of Italian Space Agency that aims at developing modular multipurpose mini-satellite platforms that can accommodate payloads of different sizes. It consists of a compact, low-cost X-band SAR payload with resolution in the order of a meter, which can operate both in monostatic and bistatic modes, exploiting one of the satellites of the COSMO-SkyMed Second Generation (CSG) constellation as illuminator. The mission foresees two operational phases. In

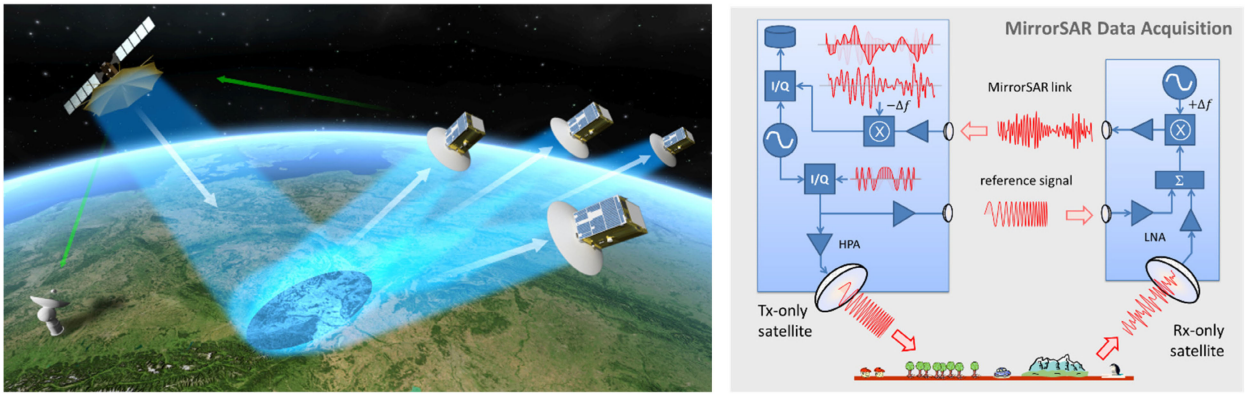

Fig. 18. ***MirrorSAR: mission implementation example with one transmitter satellite and four small satellites acting as space transponders (left) and multistatic operation and synchronization concept (right) [157], [186].***

the first phase, PLATiNO-1 will operate in nominal bistatic mode on the same orbit of CSG in a large along-track baseline formation up to about 350 km. In the second phase, the satellite will operate in nominal monostatic mode at a lower altitude of 428 km, while offering opportunities for bistatic acquisitions, with a wide range of bistatic geometries, when in conjunction with CSG. The diversity of information provided by the multiangular view will provide a significant added value compared to monostatic SAR capabilities. The PLATiNO-1 mission will provide an unprecedented opportunity to test several observation and processing techniques that leverage long baseline bistatic SAR acquisitions for the generation of novel products. The development of PLATiNO-1 mission is currently in Phase D [187].

PIESAT HongTu-1 (See Also Section IV): A further milestone in the field of multistatic SAR was the launch of the X-band SAR formation HongTu-1 in 2023 by Chinese company PIESAT. The overall system consists of one active monostatic SAR sensor and the three additional passive SAR receivers, which are arranged as a cartwheel in a circle around the active sensor [178]. In this way, six single-pass interferometric pairs are simultaneously obtained [188]. The acquired data allowed the demonstration of applications of multistatic coherence-based image analysis, e.g., forests can be recognized by their reduced single-pass coherence values. The multistatic coherence and its dependence on the interferometric baseline can, therefore, be used to estimate parameters related to forest biomass [189]. Further launches of the four-satellite multistatic SAR system HongTu-1 took place in November and December 2024. Another launch is planned, bringing the total number of multistatic SAR systems in orbit to 4.

VI. CONCLUSION AND WAY FORWARD

Today, the development of spaceborne SAR is being driven by two main streams: full-fledged SAR systems funded by space agencies and NewSpace SAR funded by the private sector. These two streams are complementary in their application fields. While NewSpace SAR fills an important gap in providing highest-resolution SAR imagery with very short revisit times, focusing on reconnaissance, security, and emergency-related applications (e.g., defense and intelligence, disaster relief and crisis management, and maritime surveillance), full-fledged SAR systems aim at global Earth observation for environmental monitoring and climate research (e.g., deforestation, forest biomass, soil moisture, ground deformation, agriculture, land cover mapping, wetland, glacier and permafrost monitoring, as well as security and emergency). In fact, there is an overlap between the two classes of SAR systems in some of these applications, which is actually a complementarity that will be discussed later in this section.

Table 4 shows a comparison between NewSpace SAR and full-fledged SAR systems, with typical values at the system and mission level, which may differ depending on the specific SAR mission and technology used. In summary, NewSpace SAR offers at least two orders of magnitude shorter revisit times using a constellation of satellites, about ten times lower cost per satellite, ten times less weight, and 25 times better spatial resolution. On the other hand, full-fledged SAR systems have at least two orders of magnitude higher imaging capacity, approximately 6 dB better SNR, better image calibration (0.3 dB instead of 1–2.5 dB for NewSpace SAR), and four times longer mission lifetime due to the use of space-qualified components and higher redundancy at the system and subsystem level. NewSpace SAR also offers a high degree of tasking flexibility, i.e., image acquisition can be ordered in real time and data delivery can occur in less than an hour, while full-fledged SAR systems have a systematic image acquisition plan to ensure a coverage of large areas in a systematic and effective way although the data delivery time is typically less than a day for disaster and emergency-related applications.

NewSpace SAR satellite development today is focused almost exclusively on the X band due to the ITU frequency

Table 4 Comparison Between NewSpace SAR Constellations and Full-Fledged SAR Systems [101], [190]

Parameter	NewSpace SAR	Full-Fledged SAR Satellites
Satellite costs	US$ 10 M to 25 M	US$ 120 M to 350 M
Satellite weight	85 kg to 250 kg	500 kg to 2.5 tons
Spatial resolution	0.25 m to 25 m	5 to 100 m
Polarization	single polarization	single, dual or quadruple polarization
Noise Equivalent Sigma Zero (NESZ)	-15 dB to -19 dB	- 20 to -28 dB
Swath width	5 km to 10 km (Spotlight)	30 to 600 km (Stripmap & ScanSAR)
Coverage	Local (< 0.05 M km^2/day)	Global (0.5 to 20 M km^2/day)
Image costs per square kilometer	US$ 15	US$ 0.02
Revisit time	few hours	few days to 14 days
Lifetime	1 to 3 years	5 to 15 years
Radar frequency (band)	X	X, C, S, L or P

allocation of up to 1.2 GHz, the attractive business case for high-resolution imagery, and the small size of the SAR antenna, which reduces the cost and weight of the satellite. Looking ahead to the future development, NewSpace SAR systems will continue to focus on the X band for reconnaissance, security, and emergency-related applications, as the frequency allocation for the other remote sensing frequency bands limits the system bandwidth to a few 100 MHz or less, constraining the range resolution to the meter regime. In addition, most of the full-fledged SAR systems have an open data policy (i.e., free data distribution, such as the satellites of NASA's Earth observation program, and the Copernicus program of ESA and European Union) and already provide high-quality data in C and L bands, and in the near future also in X and P bands. For applications related to hazard monitoring and

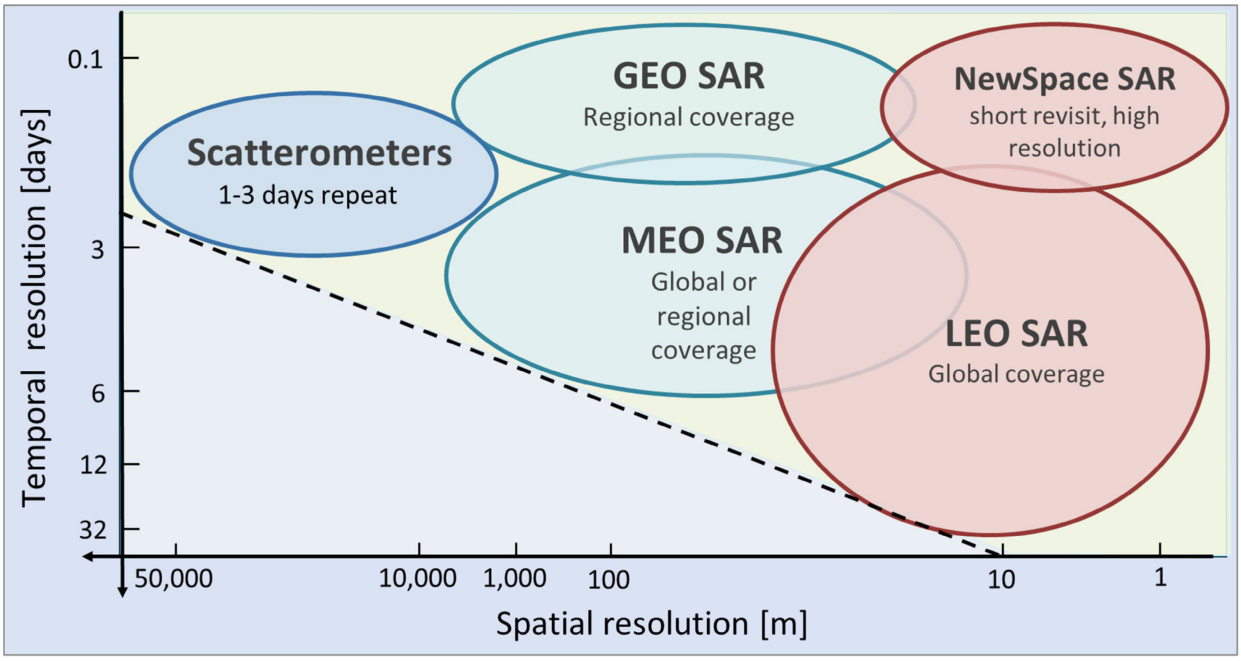

Fig. 19. *Temporal versus spatial resolution for different spaceborne SAR concepts. Different SAR system concepts are required to fill the trade space of temporal and spatial resolutions required for each user application. Scatterometers are real aperture radars [4], [5], [191], GEO SARs are geosynchronous SAR systems at 36,000-km orbit height [192], [193], [194], MEO SARs are medium Earth orbit SAR at, e.g., 6,000 km [37], LEO SARs are full-fledged SAR systems at 500–800-km orbit (see Section III), and NewSpace SARs are small satellites at 500–600-km orbit (see Section IV).*

disaster management (e.g., floods, volcanic activity, earthquake damage assessment, and landslide detection), both full-fledged and NewSpace SAR systems are important and complementary. While full-fledged SAR systems cover a large area with moderate resolution and provide an overview of the current situation, NewSpace SAR systems achieve short revisit times in the focus areas of the emergency with detailed information due to the very high spatial resolution. Therefore, exploiting the complementarity of both systems is a key aspect for the coming years. In fact, ESA's Third-Party Missions (TPMs) program and NASA's Commercial Satellite Data Acquisition (CSDA) program are already using NewSpace SAR data to complement their own satellite data.

NewSpace SAR companies such as ICEYE, Capella, Umbra, iQPS, and Synspective have revolutionized spaceborne SAR with much smaller satellites using disruptive technologies at low cost. On the other hand, full-fledged spaceborne SAR has entered a golden age with the launch of a new generation of spaceborne SAR using phased array antennas like ALOS-2 (Japan), Radarsat-2 and Radarsat Constellation Mission (Canada), COSMO-SkyMed-1/4 and COSMO-SkyMed-SG (Italy), TerraSAR-X/TanDEM-X (Germany), Sentinel-1 (ESA/EU), PAZ (Spain), KOMPSAT-5 (South Korea), RISAT-2 (India), and SAOCOM-1/2 (Argentina). A paradigm shift is taking place for full-fledged SAR systems with the introduction of DBF (see Section III). New generation SAR systems such as ALOS-4 (already in operation), NISAR (already launched), ROSE-L, Sentinel-1 NG, PAZ-2, and Kompsat-8 will have ten times the imaging capacity of conventional SAR systems with the same or even improved spatial resolution. It becomes possible to circumvent the fundamental limitation of the SAR system design and to achieve high resolution and wide swath coverage. However, the increase in image capacity provided by DBF grows with the number of receive channels, which leads to an increase in data rate. Therefore, an onboard processing, which is typically performed using an FPGA, is required to perform DBF and reduce the data rate. For a SAR system like the mission proposal Tandem-L [95], consisting of a large reflector antenna illuminated by a digital feed array, a study has been conducted to investigate the feasibility of introducing a high-resolution mode with an azimuth resolution of 1 m (at least for a part of the total swath), in addition to the standard imaging mode with a swath width of 350 km at 7-m resolution. Although DBF in azimuth would meet the 1-m azimuth resolution requirement, the complexity of the onboard signal processing for DBF and data reduction results in a high-power consumption, comparable to that of the radar system itself, with an average power consumption of a few hundred watts. On the other hand, NewSpace SAR cannot replace full-fledged SAR systems. For example, several hundred NewSpace SAR satellites would be required to replace a next-generation SAR system like Sentinel-1 NG with a 400-km swath width, 5 m $\times$ 5 m spatial resolution, and up to 40-min operation time per orbit cycle, resulting in much higher costs and overall space system complexity.

The above examples illustrate that a single radar technology does not represent the most efficient and cost-effective solution for all types of applications and user requirements. On the contrary, for each application, there will be an appropriate mission concept and technology that fulfills the user requirements in a most efficient way. Fig. 19 provides an overview of the temporal versus spatial resolution for different spaceborne SAR concepts and technologies. While scatterometers (real aperture radars [191] or unfocused SAR systems such as SMAP [195]) provide a global Earth coverage with a three-day revisit time and low resolution for the estimation of soil moisture over the land masses and/or wind speed over the ocean, LEO SAR satellites, both full-fledged and NewSpace, provide much higher resolution, as discussed earlier in this article. MEO SAR systems, although not yet being considered for realization, offer an interesting tradeoff between resolution and coverage for applications like ground deformation or soil moisture estimation [37], which requires global coverage at medium resolution. Geosynchronous Earth orbit (GEO) SAR systems enable a monitoring on a regional scale (a few to several thousand kilometers longitude and latitude extension, depending on the selected orbit) with moderate–low spatial resolution [192], [193], [194]. The only GEO SAR system in orbit today was developed in China, denoted as Ludi-Tance-4 01A [196], [197]. A study phase of a geosynchronous SAR mission proposal (Hydroterra+) is also being carried out by ESA in the scope of the 12th Earth Explorer candidate missions with a focus on applications related to weather forecast of extreme events, hydrology, mountain cryosphere, as well as ground deformation.

Multistatic and distributed SAR systems introduce a new dimension in the SAR imaging and provide additional information, novel information products, and more flexibility in the system configuration. Although today only three SAR systems, TanDEM-X (Germany), SuperView Neo 2 (China), and HongTu-1/2 (China) are operating in bistatic and multistatic modes, all required technologies and techniques, including formation flying, time and phase synchronization, bistatic calibration and signal processing, are already well-understood and mature to allow the realization of further spaceborne systems. It is expected that a rapid development will occur in the next years in this field. The combination of full-fledged SAR systems with small satellites is also very promising. In principle, any full-fledged SAR system can be augmented by small SAR satellites in formation flight to provide images with additional information content, as described in Section V. ESA's Harmony mission, to be launched in 2029, is a notable example of a multistatic SAR mission consisting of two receive-only satellites as an add-on to the successful series of the Sentinel-1 satellites [185].

In today's world, the demand for high-resolution, near real-time geospatial and environmental information with global accessibility and coverage is becoming increasingly imperative. In this context, full-fledged SAR systems with global coverage and constellations of NewSpace SAR

play a transformative role. European Union's Copernicus program, started in 2014 with the launch of Sentinel-1A, showcases several operational services, with varying degrees of maturity, which have been developed and are provided free of charge to users. Unlike optical sensors, spaceborne SAR systems are unique in providing high-resolution imagery regardless of weather conditions or daytime. Looking ahead, the vision of a space-based sensor web is not far away: a network of radar satellites capable of delivering near-real-time, high-resolution imagery with relevant information on a global scale. Advances in SAR technology, mission concepts, miniaturization, and satellite deployment are paving the way for such a system. ■

REFERENCES

[1] C. A. Wiley, "Synthetic aperture radars," *IEEE Trans. Aerosp. Electron. Syst.*, vol. AES-3, pp. 440–443, 1985.

[2] J. C. Curlander and R. N. McDonough, *Synthetic Aperture Radar*, vol. 11. New York, NY, USA: Wiley, 1991.

[3] A. Moreira, P. Prats-Iraola, M. Younis, G. Krieger, I. Hajnsek, and K. P. Papathanassiou, "A tutorial on synthetic aperture radar," *IEEE Geosci. Remote Sens. Mag.*, vol. 1, no. 1, pp. 6–43, Mar. 2013.

[4] D. Long and F. Ulaby, *Microwave Radar and Radiometric Remote Sensing*. Norwood, MA, USA: Artech House, 2015.

[5] C. Elachi and J. J. Van Zyl, *Introduction to the Physics and Techniques of Remote Sensing*. Hoboken, NJ, USA: Wiley, 2021.

[6] J. Ju and D. P. Roy, "The availability of cloud-free Landsat ETM+ data over the conterminous United States and globally," *Remote Sens. Environ.*, vol. 112, no. 3, pp. 1196–1211, Mar. 2008.

[7] G. P. Asner, "Cloud cover in Landsat observations of the Brazilian Amazon," *Int. J. Remote Sens.*, vol. 22, no. 18, pp. 3855–3862, Jan. 2001.

[8] P. A. Rosen et al., "Synthetic aperture radar interferometry," *Proc. IEEE*, vol. 88, no. 3, pp. 333–382, Mar. 2000.

[9] P. Berardino, G. Fornaro, R. Lanari, and E. Sansosti, "A new algorithm for surface deformation monitoring based on small baseline differential SAR interferograms," *IEEE Trans. Geosci. Remote Sens.*, vol. 40, no. 11, pp. 2375–2383, Nov. 2002.

[10] J.-S. Lee and E. Pottier, *Polarimetric Radar Imaging: From Basics to Applications*. Boca Raton, FL, USA: CRC Press, 2017.

[11] P. Escudier et al., "Satellite radar altimetry: Principle, accuracy, and precision," in *Satellite Altimetry Over Oceans and Land Surfaces*. Boca Raton, FL, USA: CRC Press, 2017, pp. 1–70.

[12] S. Gogineni et al., "Coherent radar ice thickness measurements over the Greenland ice sheet," *J. Geophys. Res., Atmos.*, vol. 106, no. D24, pp. 33761–33772, Dec. 2001.

[13] R. Jordan, "The seasat—A synthetic aperture radar system," *IEEE J. Ocean. Eng.*, vol. OE-5, no. 2, pp. 154–164, Apr. 1980.

[14] *EoPortal: Satellite Missions*. Accessed: Apr. 24, 2025. [Online]. Available: https://www.eoportal.org/satellite-missions/ers-1#eop-quick-facts-section

[15] M. Shimada, "Radiometric and geometric calibration of JERS-1 SAR," *Adv. Space Res.*, vol. 17, no. 1, pp. 79–88, 1996.

[16] A. Freeman, M. Zink, E. Caro, A. Moreira, L. Veilleux, and M. Werner, "The legacy of the SIR-C/X-SAR radar system: 25 years on," *Remote Sens. Environ.*, vol. 231, Sep. 2019, Art. no. 111255.

[17] R. Werninghaus and S. Buckreuss, "The TerraSAR-X mission and system design," *IEEE Trans. Geosci. Remote Sens.*, vol. 48, no. 2, pp. 606–614, Feb. 2010.

[18] F. Covello et al., "COSMO-SkyMed an existing opportunity for observing the Earth," *J. Geodynamics*, vol. 49, nos. 3–4, pp. 171–180, Apr. 2010.

[19] L. C. Morena, K. V. James, and J. Beck, "An introduction to the RADARSAT-2 mission," *Can. J. Remote Sens.*, vol. 30, no. 3, pp. 221–234, Jan. 2004.

[20] M. Zink et al., "TanDEM-X: 10 years of formation flying bistatic SAR interferometry," *IEEE J. Sel. Topics Appl. Earth Observ. Remote Sens.*, vol. 14, pp. 3546–3565, 2021.

[21] R. Torres et al., "Sentinel-1 SAR system and mission," in *Proc. IEEE Radar Conf. (RadarConf)*, May 2017, pp. 1582–1585.

[22] B. Chapman and R. G. Blom, "Synthetic aperture radar, technology, past and future applications to archaeology," in *Mapping Archaeological Landscapes From Space* (Springer Briefs in Archaeology), vol. 5. New York, NY, USA: Springer, 2013, pp. 113–131.

[23] D. B. Campbell et al., "Magellan observations of extended impact Crater related features on the surface of Venus," *J. Geophys. Res., Planets*, vol. 97, no. E10, pp. 16249–16277, Oct. 1992.

[24] A. Le Gall et al., "Cassini SAR, radiometry, scatterometry and altimetry observations of Titan's dune fields," *Icarus*, vol. 213, no. 2, pp. 608–624, Jun. 2011.

[25] F. Henderson and A. Lewis, *Manual of Remote Sensing: Principles and Applications of Imaging Radar*. New York, NY, USA: Wiley, 1998.

[26] W. Emery and A. Camps, *Introduction to Satellite Remote Sensing: Atmosphere, Ocean, Land and Cryosphere Applications*. Amsterdam, The Netherlands: Elsevier, 2017.

[27] W. G. Carrara, R. S. Goodman, and R. M. Majewski, *Spotlight Synthetic Aperture Radar: Signal Processing Algorithms (IPF)*. Norwood, MA, USA: Artech House, 1995.

[28] G. Franceschetti and R. Lanari, *Synthetic Aperture Radar Processing*. Boca Raton, FL, USA: CRC Press, 1999.

[29] I. G. Cumming and F. H. Wong, *Digital Processing of Synthetic Aperture Radar Data: Algorithms and Implementation*. Norwood, MA, USA: Artech House, 2005.

[30] R. K. Raney, H. Runge, R. Bamler, I. G. Cumming, and F. H. Wong, "Precision SAR processing using chirp scaling," *IEEE Trans. Geosci. Remote Sens.*, vol. 32, no. 4, pp. 786–799, Jul. 1994.

[31] A. Moreira, J. Mittermayer, and R. Scheiber, "Extended chirp scaling algorithm for air- and spaceborne SAR data processing in stripmap and ScanSAR imaging modes," *IEEE Trans. Geosci. Remote Sens.*, vol. 34, no. 5, pp. 1123–1136, Sep. 1996.

[32] F. K. Li and W. T. K. Johnson, "Ambiguities in spacebornene synthetic aperture radar systems," *IEEE Trans. Aerosp. Electron. Syst.*, vol. AES-19, no. 3, pp. 389–397, May 1983.

[33] K. Tomiyasu, "Conceptual performance of a satellite borne, wide swath synthetic aperture radar," *IEEE Trans. Geosci. Remote Sens.*, vol. GRS-19, no. 2, pp. 108–116, Apr. 1981.

[34] F. De Zan and A. Monti Guarnieri, "TOPSAR: Terrain observation by progressive scans," *IEEE Trans. Geosci. Remote Sens.*, vol. 44, no. 9, pp. 2352–2360, Sep. 2006.

[35] J. Mittermayer, A. Moreira, and O. Loffeld, "Spotlight SAR data processing using the frequency scaling algorithm," *IEEE Trans. Geosci. Remote Sens.*, vol. 37, no. 5, pp. 2198–2214, Sep. 1999.

[36] P. Prats, R. Scheiber, J. Mittermayer, A. Meta, and A. Moreira, "Processing of sliding spotlight and TOPS SAR data using baseband azimuth scaling," *IEEE Trans. Geosci. Remote Sens.*, vol. 48, no. 2, pp. 770–780, Feb. 2010.

[37] J. Matar, M. Rodriguez-Cassola, G. Krieger, P. López-Dekker, and A. Moreira, "MEO SAR: System concepts and analysis," *IEEE Trans. Geosci. Remote Sens.*, vol. 58, no. 2, pp. 1313–1324, Feb. 2020.

[38] J. Van Zyl and Y. Kim, *Synthetic Aperture Radar Polarimetry*. Hoboken, NJ, USA: Wiley, 2011.

[39] I. Hajnsek and Y.-L. Desnos, Eds., *Polarimetric Synthetic Aperture Radar: Principles and Application*, vol. 25. Cham, Switzerland: Springer, 2021.

[40] Japan Aerospace Exploration Agency (JAXA). (Apr. 2021). *Advanced Land Observing Satellite-4 (ALOS-4)*. [Online]. Available: https://global.jaxa.jp/projects/sat/alos4/

[41] Jet Propulsion Laboratory (JPL). (Jul. 2022). *The NASA ISRO SAR Mission NISAR: Quick Facts*. [Online]. Available: https://nisar.jpl.nasa.gov

[42] P. Rosen et al., "The NASA-ISRO SAR (NISAR) mission dual-band radar instrument preliminary design," in *Proc. IEEE Int. Geosci. Remote Sens. Symp. (IGARSS)*, Fort Worth, TX, USA, Jul. 2017, pp. 3832–3835.

[43] R. Torres et al., "Sentinel-1 next generation: Enhanced C-band data continuity," in *Proc. 14th Eur. Conf. Synth. Aperture Radar (EUSAR)*, Munich, Germany, Jul. 2022, pp. 1–3.

[44] M. Davidson, N. Gebert, and L. Giulicchi, "ROSE-L—The L-band SAR mission for Copernicus," in *Proc. 13th Eur. Conf. Synth. Aperture Radar (EUSAR)*, Mar. 2021, pp. 1–2.

[45] F. Rostan et al., "ROSE-L SAR instrument design overview and performance," in *Proc. Eur. Conf. Synth. Aperture Radar (EUSAR)*, Munich, Germany, Apr. 2024, pp. 209–214.

[46] C. Fischer, C. Schaefer, and C. Heer, "Digital beamforming antenna for synthetic aperture radar," in *Proc. 2nd Eur. Conf. Antennas Propag. (EuCAP)*, Edinburgh, U.K., 2007, p. 520.

[47] J. Janoth, M. Jochum, L. Petrat, and T. Knigge, "High resolution wide swath—The next generation X-band mission," in *Proc. IEEE Int. Geosci. Remote Sens. Symp. (IGARSS)*, Yokohama, Japan, Jul. 2019, pp. 3535–3537.

[48] A. Freeman et al., "The 'Myth' of the minimum SAR antenna area constraint," *IEEE Trans. Geosci. Remote Sens.*, vol. 38, no. 1, pp. 320–324, Jan. 2000.

[49] H. D. Griffiths and P. Mancini, "Ambiguity suppression in SARs using adaptive array techniques," in *Proc. IGARSS*, vol. 2, Dec. 1991, pp. 1015–1018.

[50] A. Currie and M. A. Brown, "Wide-swath SAR," *IEE Proc. F-Radar Signal Process.*, vol. 139, no. 2, pp. 122–155, 1992.

[51] G. D. Callaghan and I. D. Longstaff, "Wide-swath space-borne SAR using a quad-element array," *IEE Proc.-Radar, Sonar Navigat.*, vol. 146, no. 3, pp. 159–165, 1999.

[52] G. D. Callaghan, "Wide-swath space-borne SAR: Overcoming the trade-off between swath-width and resolution," Ph.D. dissertation, University of Queensland, Brisbane, QLD, Australia, 1999.

[53] M. Suess, B. Grafmueller, and R. Zahn, "A novel high resolution, wide swath SAR system," in *Proc. IEEE Int. Geosci. Remote Sens. Symp. (IGARSS)*, vol. 3, Sydney, NSW, Australia, Aug. 2001, pp. 1013–1015.

[54] M. Süß and W. Wiesbeck, "Side-looking synthetic aperture radar system," E.P. Patent 1 241 487, Sep. 18, 2002.

[55] M. Younis, C. Fischer, and W. Wiesbeck, "Digital beamforming in SAR systems," *IEEE Trans. Geosci. Remote Sens.*, vol. 41, no. 7,

pp. 1735–1739, Jul. 2003.
[56] G. Krieger, N. Gebert, and A. Moreira, "Unambiguous SAR signal reconstruction from nonuniform displaced phase center sampling," *IEEE Geosci. Remote Sens. Lett.*, vol. 1, no. 4, pp. 260–264, Oct. 2004.
[57] G. Krieger, N. Gebert, and A. Moreira, "Multidimensional waveform encoding: A new digital beamforming technique for synthetic aperture radar remote sensing," *IEEE Trans. Geosci. Remote Sens.*, vol. 46, no. 1, pp. 31–46, Jan. 2008.
[58] N. Gebert, G. Krieger, and A. Moreira, "Digital beamforming on receive: Techniques and optimization strategies for high-resolution wide-swath SAR imaging," *IEEE Trans. Aerosp. Electron. Syst.*, vol. 45, no. 2, pp. 564–592, Apr. 2009.
[59] N. Gebert, "Multi-channel azimuth processing for high-resolution wide-swath SAR imaging," Ph.D. dissertation, Dept. Radar Concepts, Microw. Radar Inst., German Aerosp. Center (DLR), Cologne, Germany, Aug. 2009.
[60] J.-H. Kim, M. Younis, P. Prats-Iraola, M. Gabele, and G. Krieger, "First spaceborne demonstration of digital beamforming for azimuth ambiguity suppression," *IEEE Trans. Geosci. Remote Sens.*, vol. 51, no. 1, pp. 579–590, Jan. 2013.
[61] M. Younis, P. Lopez-Dekker, F. Bordoni, P. Laskowski, and G. Krieger, "Exploring the trade-space of MIMO SAR," in *Proc. IEEE Int. Geosci. Remote Sens. Symp.-IGARSS*, Melbourne, VIC, Australia, Jul. 2013, pp. 4455–4458.
[62] M. Younis, F. Q. D. Almeida, P. Lopez-Dekker, and G. Krieger, "Techniques and modes for multi-channel SAR instruments," in *Proc. 11th Eur. Conf. Synth. Aperture Radar (EUSAR)*, Hamburg, Germany, Jun. 2016, pp. 1–6.
[63] G. Krieger, "MIMO-SAR: Opportunities and pitfalls," *IEEE Trans. Geosci. Remote Sens.*, vol. 52, no. 5, pp. 2628–2645, May 2014.
[64] M. Villano, G. Krieger, M. Jäger, and A. Moreira, "Staggered SAR: Performance analysis and experiments with real data," *IEEE Trans. Geosci. Remote Sens.*, vol. 55, no. 11, pp. 6617–6638, Nov. 2017.
[65] F. He, X. Ma, Z. Dong, and D. Liang, "Digital beamforming on receive in elevation for multidimensional waveform encoding SAR sensing," *IEEE Geosci. Remote Sens. Lett.*, vol. 11, no. 12, pp. 2173–2177, Dec. 2014.
[66] J.-H. Kim, M. Younis, A. Moreira, and W. Wiesbeck, "Spaceborne MIMO synthetic aperture radar for multimodal operation," *IEEE Trans. Geosci. Remote Sens.*, vol. 53, no. 5, pp. 2453–2466, May 2015.
[67] F. Zhou, G. Shen, Y. Liu, J. Fang, J. Zhang, and M. Xing, "Simultaneous multiresolution imaging based on multimode MIMO-SAR," *IEEE J. Sel. Topics Appl. Earth Observ. Remote Sens.*, vol. 16, pp. 8456–8474, 2023.
[68] J. del Castillo, S. Sánchez, R. de Porras, A. Pedreira, and J. R. Larrañaga, "L-band digital array radar demonstrator for next generation multichannel SAR systems," *IEEE J. Sel. Topics Appl. Earth Observ. Remote Sens.*, vol. 8, no. 11, pp. 5007–5014, Nov. 2015.
[69] Q. Garcia et al., "Hybrid analog-digital SAR instrument with reflector antenna and overlapped subarray feed for Earth observation," *IEEE Antennas Wireless Propag. Lett.*, vol. 20, no. 11, pp. 2110–2114, Nov. 2021.
[70] J. H. Blythe, "Radar systems," U.S. Patent 4 253 098, Feb. 24, 1981.
[71] J. T. Kare, "Moving receive beam method and apparatus for synthetic aperture radar," U.S. Patent 6 175 326, Jan. 16, 2001.
[72] M. Younis, T. Rommel, F. Bordoni, G. Krieger, and A. Moreira, "On the pulse extension loss in digital beamforming SAR," *IEEE Geosci. Remote Sens. Lett.*, vol. 12, no. 7, pp. 1436–1440, Jul. 2015.
[73] S. Huber, M. Younis, A. Patyuchenko, G. Krieger, and A. Moreira, "Spaceborne reflector SAR systems with digital beamforming," *IEEE Trans. Aerosp. Electron. Syst.*, vol. 48, no. 4, pp. 3473–3493, Oct. 2012.
[74] M. Younis, F. Q. de Almeida, M. Villano, S. Huber, G. Krieger, and A. Moreira, "Digital beamforming for spaceborne reflector-based synthetic aperture radar, Part 1: Basic imaging modes," *IEEE Geosci. Remote Sens. Mag.*, vol. 9, no. 3, pp. 8–25, Sep. 2021.
[75] M. Younis, S. Huber, A. Patyuchenko, F. Bordoni, and G. Krieger, "Performance comparison of reflector- and planar-antenna based digital beam-forming SAR," *Int. J. Antennas Propag.*, vol. 2009, pp. 1–13, Jun. 2009.
[76] F. Q. de Almeida, T. Rommel, M. Younis, G. Krieger, and A. Moreira, "Multichannel staggered SAR: System concepts with reflector and planar antennas," *IEEE Trans. Aerosp. Electron. Syst.*, vol. 55, no. 2, pp. 877–902, Apr. 2019.
[77] D. Cerutti-Maori and I. Sikaneta, "A generalization of DPCA processing for multichannel SAR/GMTI radars," *IEEE Trans. Geosci. Remote Sens.*, vol. 51, no. 1, pp. 560–572, Jan. 2013.
[78] I. Sikaneta, C. H. Gierull, and D. Cerutti-Maori, "Optimum signal processing for multichannel SAR: With application to high-resolution wide-swath imaging," *IEEE Trans. Geosci. Remote Sens.*, vol. 52, no. 10, pp. 6095–6109, Oct. 2014.
[79] D. Cerutti-Maori, I. Sikaneta, J. Klare, and C. H. Gierull, "MIMO SAR processing for multichannel high-resolution wide-swath radars," *IEEE Trans. Geosci. Remote Sens.*, vol. 52, no. 8, pp. 5034–5055, Aug. 2014.
[80] F. Q. De Almeida, M. Younis, G. Krieger, and A. Moreira, "An analytical error model for spaceborne SAR multichannel azimuth reconstruction," *IEEE Geosci. Remote Sens. Lett.*, vol. 15, no. 6, pp. 853–857, Jun. 2018.
[81] G. Krieger et al., "SIMO and MIMO system architectures and modes for high-resolution ultra-wide-swath SAR imaging," in *Proc. 11th Eur. Conf. Synth. Aperture Radar (EUSAR)*, Hamburg, Germany, Jun. 2016, pp. 1–6.
[82] M. Younis, F. De Almeida, M. Villano, S. Huber, G. Krieger, and A. Moreira, "Digital beamforming for spaceborne reflector-based synthetic aperture radar, Part 2: Ultrawide-swath imaging mode," *IEEE Geosci. Remote Sens. Mag.*, vol. 10, no. 4, pp. 10–31, Dec. 2022.
[83] G. Krieger, N. Gebert, M. Younis, F. Bordoni, A. Patyuchenko, and A. Moreira, "Advanced concepts for ultra-wide-swath SAR imaging," in *Proc. 7th Eur. Conf. Synth. Aperture Radar (EUSAR)*, Jun. 2008, pp. 1–4.
[84] N. Gebert, G. Krieger, and A. Moreira, "Multichannel azimuth processing in ScanSAR and TOPS mode operation," *IEEE Trans. Geosci. Remote Sens.*, vol. 48, no. 7, pp. 2994–3008, Jul. 2010.
[85] M. Ludwig et al., "Earth observation instruments with e-scan antennas state-of-the-art and outlook," in *IEEE MTT-S Int. Microw. Symp. Dig.*, May 2010, pp. 1–1.
[86] A. Freeman et al., "SweepSAR: Beam-forming on receive using a reflector-phased array feed combination for spaceborne SAR," in *Proc. IEEE Radar Conf.*, Pasadena, CA, USA, May 2009, pp. 1–9.
[87] G. Krieger et al., "CEBRAS: Cross elevation beam range ambiguity suppression for high-resolution wide-swath and MIMO-SAR imaging," in *Proc. IEEE Int. Geosci. Remote Sens. Symp. (IGARSS)*, Milan, Italy, Jul. 2015, pp. 196–199.
[88] M. Villano, G. Krieger, and A. Moreira, "Nadir echo removal in synthetic aperture radar via waveform diversity and dual-focus postprocessing," *IEEE Geosci. Remote Sens. Lett.*, vol. 15, no. 5, pp. 719–723, May 2018.
[89] F. Q. de Almeida, M. Younis, P. Prats-Iraola, M. Rodriguez-Cassola, G. Krieger, and A. Moreira, "Slow pulse repetition interval variation for high-resolution wide-swath SAR imaging," *IEEE Trans. Geosci. Remote Sens.*, vol. 59, no. 7, pp. 5665–5686, Jul. 2021.
[90] B. Grafmueller and C. Schaefer, "High resolution synthetic aperture radar device and antenna for one such radar," U.S. Patent 2009/0 079 621 A1, Mar. 26, 2006.
[91] M. Villano, G. Krieger, and A. Moreira, "Staggered SAR: High-resolution wide-swath imaging by continuous PRI variation," *IEEE Trans. Geosci. Remote Sens.*, vol. 52, no. 7, pp. 4462–4479, Jul. 2014.
[92] M. Villano, G. Krieger, and A. Moreira, "A novel processing strategy for staggered SAR," *IEEE Geosci. Remote Sens. Lett.*, vol. 11, no. 11, pp. 1891–1895, Nov. 2014.
[93] M. Villano, G. Krieger, and A. Moreira, "Onboard processing for data volume reduction in high-resolution wide-swath SAR," *IEEE Geosci. Remote Sens. Lett.*, vol. 13, no. 8, pp. 1173–1177, Aug. 2016.
[94] H. Huang et al., "A novel method for staggered SAR imaging in an elevation multichannel system," *IEEE Trans. Geosci. Remote Sens.*, vol. 61, 2023, Art. no. 5100919.
[95] A. Moreira et al., "Tandem-L: A highly innovative bistatic SAR mission for global observation of dynamic processes on the Earth's surface," *IEEE Geosci. Remote Sens. Mag.*, vol. 3, no. 2, pp. 8–23, Jun. 2015.
[96] S. Huber, F. Q. de Almeida, M. Villano, M. Younis, G. Krieger, and A. Moreira, "Tandem-L: A technical perspective on future spaceborne SAR sensors for Earth observation," *IEEE Trans. Geosci. Remote Sens.*, vol. 56, no. 8, pp. 4792–4807, Aug. 2018.
[97] F. Q. De Almeida, M. Younis, G. Krieger, and A. Moreira, "Multichannel staggered SAR azimuth processing," *IEEE Trans. Geosci. Remote Sens.*, vol. 56, no. 5, pp. 2772–2788, May 2018.
[98] M. Villano, J. Márquez-Martínez, D. Moller, and M. Younis, "Overview of newspace synthetic aperture radar instrument activities," in *Proc. IGARSS-IEEE Int. Geosci. Remote Sens. Symp.*, Kuala Lumpur, Malaysia, Jul. 2022, pp. 4130–4132.
[99] K. Davidian, "Definition of NewSpace," *New Space*, vol. 8, no. 2, pp. 53–55, Jun. 2020, doi: 10.1089/space.2020.29027.kda.
[100] ICEYE. (Jan. 17, 2018). *First ICEYE-X1 Radar Image From Space Published*. Accessed: Feb. 26, 2025. [Online]. Available: https://www.iceye.com/press/press-releases/first-iceye-x1-radar-image-from-space-published
[101] S. A. Huang et al., "A new age of SAR: How can commercial smallsat constellations contribute to NASA's surface deformation and change mission?" *Earth Space Sci.*, vol. 12, no. 1, Jan. 2025, Art. no. e2024EA003832.
[102] NewSpace Index. *SAR (Synthetic Aperture Radar) Constellations*. Accessed: Mar. 28, 2025. [Online]. Available: https://www.newspace.im/
[103] ICEYE. *The ICEYE Fleet*. NewSpace Index. Accessed: Feb. 26, 2025. [Online]. Available: https://sar.iceye.com/5.2.7/productguide/fleet/
[104] ICEYE. *ICEYE Expands Its Earth Observation Capabilities With Launch of Two SAR Satellites for Mid-Inclination Orbit on the Bandwagon-2 Mission With SpaceX*. Accessed: Feb. 26, 2025. [Online]. Available: https://www.iceye.com/press/press-releases/iceye-expands-its-earth-observation-capabilities-with-launch-of-two-sar-satellites-for-mid-inclination-orbit-on-the-bandwagon-2-mission-with-spacex
[105] eoPortal. *Capella Space X-Band Synthetic Aperture Radar*. Accessed: Feb. 26, 2025. [Online]. Available: https://www.eoportal.org/satellite-missions/capella-x-sar
[106] ICEYE. *Accurate, Near Real-Time Earth Monitoring With SAR Data*. Accessed: Feb. 26, 2025. [Online]. Available: https://www.iceye.com/hubfs/Downloadables/SAR_Data_Brochure_ICEYE.pdf
[107] *ICEYE Expands Its SAR Imaging Capabilities With the Launch of Scan Wide Mode*. Accessed: Oct. 1, 2025. [Online]. Available: https://www.iceye.com/newsroom/press-

releases/iceye-expands-its-sar-imaging-capabilities-with-the-launch-of-scan-wide-mode

[108] Capella Space. *SAR Imagery Products Guide*. Accessed: Feb. 26, 2025. [Online]. Available: https://support.capellaspace.com/sar-imagery-products-guide

[109] Umbra. *Umbra Product Guide*. Accessed: Feb. 26, 2025. [Online]. Available: https://help.umbra.space/product-guide

[110] Synspective. *SAR Data Product Guide*. Accessed: Feb. 26, 2025. [Online]. Available: https://synspective.com/document/2025/sar_data_product_guide-2/

[111] G. Farquharson et al., "The new capella space satellite generation: Acadia," in *Proc. IGARSS-IEEE Int. Geosci. Remote Sens. Symp.*, Pasadena, CA, USA, Jul. 2023, pp. 1513–1516.

[112] S. Doody, M. Cohen, and J. Marquez-Martinez, "Next generation low cost space SAR developments," in *Proc. 11th Eur. Conf. Synth. Aperture Radar (EUSAR)*, Hamburg, Germany, Jun. 2016, pp. 1–5.

[113] M. Villano, G. Krieger, and A. Moreira, "Waveform-encoded SAR: A novel concept for nadir echo and range ambiguity suppression," in *Proc. 12th Eur. Conf. Synth. Aperture Radar (EUSAR)*, Jun. 2018, pp. 1–6.

[114] O. Dogan et al., "Double dual focusing for range ambiguity suppression—Experimental results," in *Proc. 14th Eur. Conf. Synth. Aperture Radar (EUSAR)*, Leipzig, Germany, Jul. 2022, pp. 1–6.

[115] A. Radius et al., "Phase variant analysis algorithm for azimuth ambiguity detection," in *Proc. IEEE Radar Conf. (RadarConf22)*, New York City, NY, USA, Mar. 2022, pp. 1–4.

[116] N. Ustalli and M. Villano, "High-resolution wide-swath ambiguous synthetic aperture radar modes for ship monitoring," *Remote Sens.*, vol. 14, no. 13, p. 3102, Jun. 2022.

[117] N. Ustalli, M. N. Peixoto, T. Kraus, U. Steinbrecher, G. Krieger, and M. Villano, "Experimental demonstration of staggered ambiguous SAR mode for ship monitoring with TerraSAR-X," *IEEE Trans. Geosci. Remote Sens.*, vol. 61, 2023, Art. no. 5221816.

[118] C. J. Ho, C. W. Tan, E. Tan, and Y. S. Lim, "TeLEOS-2 overview and initial results," in *Proc. 15th Eur. Conf. Synth. Aperture Radar (EUSAR)*, Munich, Germany, Oct. 2024, pp. 1313–1317.

[119] M. Cherniakov, Ed., *Bistatic Radar: Emerging Technology*. Hoboken, NJ, USA: Wiley, 2008.

[120] G. Krieger and A. Moreira, "Spaceborne bi-and multistatic SAR: Potential and challenges," *IEE Proc.-Radar, Sonar Navigat.*, vol. 153, no. 3, pp. 184–198, 2006.

[121] P. Dubois-Fernandez et al., "ONERA-DLR bistatic SAR campaign: Planning, data acquisition, and first analysis of bistatic scattering behaviour of natural and urban targets," *IEE Proc.-Radar, Sonar Navigat.*, vol. 153, no. 3, pp. 214–223, 2006.

[122] M. Rodriguez-Cassola et al., "First bistatic spaceborne SAR experiments with TanDEM-X," *IEEE Geosci. Remote Sens. Lett.*, vol. 9, no. 1, pp. 33–37, Jan. 2012.

[123] I. Walterscheid, J. H. G. Ender, A. R. Brenner, and O. Loffeld, "Bistatic SAR processing and experiments," *IEEE Trans. Geosci. Remote Sens.*, vol. 44, no. 10, pp. 2710–2717, Oct. 2006.

[124] M. Rodriguez-Cassola, S. V. Baumgartner, G. Krieger, and A. Moreira, "Bistatic TerraSAR-X/F-SAR spaceborne–airborne SAR experiment: Description, data processing, and results," *IEEE Trans. Geosci. Remote Sens.*, vol. 48, no. 2, pp. 781–794, Feb. 2010.

[125] M. Stefko, S. Leinss, O. Frey, and I. Hajnsek, "Coherent backscatter enhancement in bistatic Ku- and X-band radar observations of dry snow," *Cryosphere*, vol. 16, no. 7, pp. 2859–2879, Jul. 2022.

[126] R. J. Burkholder, L. J. Gupta, and J. T. Johnson, "Comparison of monostatic and bistatic radar images," *IEEE Antennas Propag. Mag.*, vol. 45, no. 3, pp. 41–50, Mar. 2003.

[127] P. Liang and L. Pierce, "Application of bistatic MIMICS to forest canopies," in *Proc. IEEE Int. Geosci. Remote Sens. Symp. (IGARSS)*, vol. 6, Anchorage, AK, USA, Nov. 2004, pp. 4328–4331.

[128] F. T. Ulaby, T. E. Van Deventer, J. R. East, T. F. Haddock, and M. E. Colluzi, "Millimeter-wave bistatic scattering from ground and vegetation targets," *IEEE Trans. Geosci. Remote Sens.*, vol. 26, no. 3, pp. 229–243, May 1988.

[129] J. P. Aguttes, "The SAR train concept: Required antenna area distributed over N smaller satellites, increase of performance by N," in *Proc. IEEE Int. Geosci. Remote Sens. Symp. (IGARSS)*, vol. 1, Aug. 2003, pp. 542–544.

[130] J. Mittermayer, G. Krieger, and M. Villano, "Multistatic dispersed swarm configurations for synthetic aperture radar imaging," *IEEE Geosci. Remote Sens. Lett.*, vol. 19, pp. 1–5, 2022.

[131] D. Giudici, P. Guccione, M. Manzoni, A. M. Guarnieri, and F. Rocca, "Compact and free-floating satellite MIMO SAR formations," *IEEE Trans. Geosci. Remote Sens.*, vol. 60, 2022, Art. no. 1000212.

[132] C. Prati and F. Rocca, "Improving slant-range resolution with multiple SAR surveys," *IEEE Trans. Aerosp. Electron. Syst.*, vol. 29, no. 1, pp. 135–143, 1993.

[133] P. M. Nguyen, M. Rodriguez-Cassola, and G. Krieger, "Analysis of elevation-based distributed SAR imaging concepts," in *Proc. 13th Eur. Conf. Synth. Aperture Radar (EUSAR)*, Mar. 2021, pp. 1–6.

[134] K. Sarabandi, J. Kellndorfer, and L. Pierce, "GLORIA: Geostationary/low-Earth orbiting radar image acquisition system: A multi-static GEO/LEO synthetic aperture radar satellite constellation for Earth observation," in *Proc. IEEE Int. Geosci. Remote Sens. Symp. (IGARSS)*, vol. 2, Toulouse, France, Aug. 2003, pp. 773–775.

[135] R. Bamler and P. Hartl, "Synthetic aperture radar interferometry," *Inverse Problems*, vol. 14, no. 4, pp. 1–54, 1998.

[136] S. Madsen and H. A. Zebker, "Imaging radar interferometry," in *Principles and Applications of Imaging Radar, Manual of Remote Sensing*, vol. 2. Hoboken, NJ, USA: Wiley, 1998, pp. 359–380.

[137] D. Massonnet and K. L. Feigl, "Radar interferometry and its application to changes in the Earth's surface," *Rev. Geophys.*, vol. 36, no. 4, pp. 441–500, Nov. 1998.

[138] R. Hanssen, *Radar Interferometry: Data Interpretation and Error Analysis*. Boston, MA, USA: Kluwer, 2001.

[139] A. Reigber and A. Moreira, "First demonstration of airborne SAR tomography using multibaseline L-band data," *IEEE Trans. Geosci. Remote Sens.*, vol. 38, no. 5, pp. 2142–2152, May 2000.

[140] G. Krieger et al., "TanDEM-X: A satellite formation for high-resolution SAR interferometry," *IEEE Trans. Geosci. Remote Sens.*, vol. 45, no. 11, pp. 3317–3341, Nov. 2007.

[141] M. Zink et al., "TanDEM-X: The new global DEM takes shape," *IEEE Geosci. Remote Sens. Mag.*, vol. 2, no. 2, pp. 8–23, Jun. 2014.

[142] G. Krieger et al., "TanDEM-X: A radar interferometer with two formation-flying satellites," *Acta Astronautica*, vol. 89, pp. 83–98, Aug. 2013.

[143] D. Cerutti-Maori and J. H. G. Ender, "Performance analysis of multistatic configurations for spaceborne GMTI based on the auxiliary beam approach," *IEE Proc.-Radar, Sonar Navigat.*, vol. 153, no. 2, pp. 96–103, 2006.

[144] A. Moreira, G. Krieger, and J. Mittermayer, "Satellite configuration for interferometric and/or tomographic remote sensing by means of synthetic aperture radar (SAR)," U.S. Patent 6 677 884, Jul. 1, 2002.

[145] F. Scala, G. Krieger, and M. Villano, "Investigation of fixed across-track baselines for distributed spaceborne SAR systems," in *Proc. Eur. Synth. Aperture Radar Conf. (EUSAR)*, Apr. 2024, pp. 32–37.

[146] J. Hueso González et al., "Bistatic system and baseline calibration in TanDEM-X to ensure the global digital elevation model quality," *ISPRS J. Photogramm. Remote Sens.*, vol. 73, pp. 3–11, Sep. 2012.

[147] J. L. Auterman, "Phase stability requirements for a bistatic SAR," in *Proc. IEEE Nat. Radar Conf.*, Atlanta, GA, USA, Oct. 1984, pp. 48–52.

[148] Q. Lin, S. Li, and W. Yu, "Review on phase synchronization methods for spaceborne multistatic synthetic aperture radar," *Sensors*, vol. 24, no. 10, p. 3122, May 2024.

[149] M. Eineder, "Oscillator clock drift compensation in bistatic interferometric SAR," in *Proc. IEEE Int. Geosci. Remote Sens. Symp. (IGARSS)*, vol. 3, Toulouse, France, Jul. 2003, pp. 1449–1451.

[150] M. Younis, R. Metzig, and G. Krieger, "Performance prediction of a phase synchronization link for bistatic SAR," *IEEE Geosci. Remote Sens. Lett.*, vol. 3, no. 3, pp. 429–433, Jul. 2006.

[151] H. Zhang, K. Liu, D. Liu, Y. Jiao, R. Wang, and D. Liang, "Non-interrupted phase synchronization scheme for LuTan-1 mission," in *Proc. 14th Eur. Conf. Synth. Aperture Radar (EUSAR)*, Leipzig, Germany, Jul. 2022, pp. 1–4.

[152] V. Candelier, P. Canzian, J. Lamboley, M. Brunet, and G. Santarelli, "Space qualified 5MHz ultra stable oscillators," in *Proc. IEEE Int. Freq. Control Symp. PDA Exhib. 17th Eur. Freq. Time Forum*, Tampa, FL, USA, Sep. 2003, pp. 575–582.

[153] Z. He, F. He, J. Chen, H. Huang, and D. Liang, "Phase synchronization processing method for alternating bistatic mode in distributed SAR," *J. Syst. Eng. Electron.*, vol. 24, no. 3, pp. 410–416, Jun. 2013.

[154] E. Rodrigues-Silva, M. Rodriguez-Cassola, A. Moreira, G. Krieger, and S. Thoelert, "Proof-of-concept of GNSS-based phase synchronization for bistatic and multistatic SAR missions," in *Proc. Eur. Conf. Synth. Aperture Radar (EUSAR)*, Nov. 2024, pp. 131–136.

[155] M. Rodriguez-Cassola, E. R. Silva Filho, P. Prats, G. Krieger, and A. Moreira, "A robust data-based clock synchronisation algorithm for multi-channel SAR systems," in *Proc. IGARSS-IEEE Int. Geosci. Remote Sens. Symp.*, Pasadena, CA, USA, Jul. 2023, pp. 7852–7855.

[156] G. Krieger et al., "Mirror-SAR: An advanced multistatic MIMO-SAR for high-resolution wide-swath Earth system monitoring," in *Proc. IEEE Int. Geosci. Remote Sens. Symp. (IGARSS)*, Fort Worth, TX, USA, Aug. 2017, pp. 23–28.

[157] G. Krieger, M. Zonno, J. Mittermayer, A. Moreira, S. Huber, and M. Rodriguez-Cassola, "MirrorSAR: A fractionated space transponder concept for the implementation of low-cost multistatic SAR missions," in *Proc. 12th Eur. Conf. Synth. Aperture Radar (EUSAR)*, Aachen, Germany, Jun. 2018, pp. 1–6.

[158] N. Ustalli, M. Villano, G. Krieger, and J. Mittermayer, "A phase synchronization technique for multistatic SAR systems based on a microwave link," in *Proc. 8th Asia–Pacific Conf. Synth. Aperture Radar (APSAR)*, Bali, Indonesia, Oct. 2023, pp. 1–6.

[159] M. Rodriguez-Cassola, P. Prats, G. Krieger, and A. Moreira, "Efficient time-domain image formation with precise topography accommodation for general bistatic SAR configurations," *IEEE Trans. Aerosp. Electron. Syst.*, vol. 47, no. 4, pp. 2949–2966, Oct. 2011.

[160] M. Villano and G. Krieger, "Impact of azimuth ambiguities on interferometric performance," *IEEE Geosci. Remote Sens. Lett.*, vol. 9, no. 5, pp. 896–900, Sep. 2012.

[161] D. Richter, M. Rodriguez-Cassola, M. Zonno, and P. Prats-Iraola, "Coherent azimuth ambiguity suppression based on linear optimum filtering of short along-track baseline SAR interferograms," in *Proc. 14th Eur. Conf. Synth. Aperture Radar (EUSAR)*, Leipzig, Germany, Jul. 2022, pp. 1–5.

[162] M. Villano, M. N. Peixoto, N. Ustalli, J. Mittermayer, G. Krieger, and A. Moreira, "Decorrelating ambiguities in SAR interferometry through slight PRI variation," *IEEE*

Trans. Geosci. Remote Sens., vol. 60, 2022, Art. no. 5240413.
[163] R. M. Goldstein and H. A. Zebker, "Interferometric radar measurement of ocean surface currents," *Nature*, vol. 328, no. 6132, pp. 707–709, Aug. 1987.
[164] F. Lombardini, F. Bordoni, F. Gini, and L. Verrazzani, "Multibaseline ATI-SAR for robust ocean surface velocity estimation," *IEEE Trans. Aerosp. Electron. Syst.*, vol. 40, no. 2, pp. 417–433, Apr. 2004.
[165] P. Prats-Iraola, P. Lopez-Dekker, F. De Zan, N. Yague-Martinez, M. Zonno, and M. Rodriguez-Cassola, "Performance of 3-D surface deformation estimation for simultaneous squinted SAR acquisitions," *IEEE Trans. Geosci. Remote Sens.*, vol. 56, no. 4, pp. 2147–2158, Apr. 2018.
[166] Y. Li, P. L. Dekker, G. Mulder, L. Iannini, and P. Prats-Iraola, "Differential tropospheric delay estimation by simultaneous multi-angle repeat-pass InSAR," *IEEE Trans. Geosci. Remote Sens.*, vol. 60, pp. 1–18, 2021.
[167] M. Lachaise, T. Fritz, and R. Bamler, "The dual-baseline phase unwrapping correction framework for the TanDEM-X mission Part 1: Theoretical description and algorithms," *IEEE Trans. Geosci. Remote Sens.*, vol. 56, no. 2, pp. 780–798, Feb. 2018.
[168] M. Nogueira Peixoto, G. Krieger, A. Moreira, C. Waldschmidt, and M. Villano, "On the exploitation of CubeSats for highly accurate and robust single-pass SAR interferometry," *IEEE Trans. Geosci. Remote Sens.*, vol. 61, 2023, Art. no. 5217216.
[169] V. Mustieles-Perez, S. Kim, G. Krieger, and M. Villano, "New insights into wideband synthetic aperture radar interferometry," *IEEE Geosci. Remote Sens. Lett.*, vol. 21, pp. 1–5, 2024.
[170] M. N. Peixoto et al., "Distributed SAR interferometry for digital elevation model generation using microsatellites: Processing and demonstration," *IEEE Trans. Geosci. Remote Sensing*, submitted for publication.
[171] K. P. Papathanassiou and S. R. Cloude, "Single-baseline polarimetric SAR interferometry," *IEEE Trans. Geosci. Remote Sens.*, vol. 39, no. 11, pp. 2352–2363, Nov. 2001.
[172] S. Tebaldini, M. Manzoni, L. Ferro-Famil, F. Banda, and D. Giudici, "FDM MIMO spaceborne SAR tomography by minimum redundancy wavenumber illumination," *IEEE Trans. Geosci. Remote Sens.*, vol. 62, 2024, Art. no. 5207119.
[173] G. Krieger, T. Rommel, and A. Moreira, "MIMO-SAR tomography," in *Proc. 11th Eur. Conf. Synth. Aperture Radar (EUSAR)*, Jun. 2016, pp. 1–6.
[174] O. Ponce, P. Prats-Iraola, R. Scheiber, A. Reigber, and A. Moreira, "First airborne demonstration of holographic SAR tomography with fully polarimetric multicircular acquisitions at L-band," *IEEE Trans. Geosci. Remote Sens.*, vol. 54, no. 10, pp. 6170–6196, Oct. 2016.
[175] A. Moccia, G. Rufino, M. D'Errico, G. Alberti, and G. Salzillo, "BISSAT: A bistatic SAR for Earth observation," in *Proc. IEEE Int. Geosci. Remote Sens. Symp.*, vol. 5, Toronto, ON, Canada, Oct. 2002, pp. 2628–2630.
[176] C. Bielski et al., "Novel approach for ranking DEMs: Copernicus DEM improves one arc second open global topography," *IEEE Trans. Geosci. Remote Sens.*, vol. 62, 2024, Art. no. 4503922.
[177] *Copernicus DEM—Global and European Digital Elevation Model*. Accessed: Apr. 1, 2025. [Online]. Available: https://dataspace.copernicus.eu/explore-data/data-collections/copernicus-contributing-missions/collections-description/COP-DEM
[178] D. Massonnet, "Capabilities and limitations of the interferometric cartwheel," *IEEE Trans. Geosci. Remote Sens.*, vol. 39, no. 3, pp. 506–520, Mar. 2001.
[179] N. Gebert, B. Carnicero Dominguez, M. W. J. Davidson, M. Diaz Martin, and P. Silvestrin, "SAOCOM-CS—A passive companion to SAOCOM for single-pass L-band SAR interferometry," in *Proc. 10th Eur. Conf. Synth. Aperture Radar (EUSAR)*, Jun. 2014, pp. 1–4.
[180] I. Hajnsek et al., "The Ka-band interferometric radar mission proposal for cold environments—SKADI," in *Proc. ESA Living Planet Symp.*, Bonn, Germany, 2022, pp. 1–7.
[181] I. Hajnsek et al., "TanDEM-X: The 4D mission phase for Earth surface dynamics: Science activities highlights and new data products after 15 years of bistatic operations," *IEEE Geosci. Remote Sens. Mag.*, vol. 13, no. 2, pp. 116–151, Jun. 2025.
[182] D. Moller et al., "Validation of glacier topographic acquisitions from an airborne single-pass interferometer," *Sensors*, vol. 19, no. 17, p. 3700, Aug. 2019.
[183] S. Hensley, D. Moller, S. Oveisgharan, T. Michel, and X. Wu, "Ka-band mapping and measurements of interferometric penetration of the Greenland ice sheets by the GLISTIN radar," *IEEE J. Select. Topics Appl. Earth Observ. Remote Sens.*, vol. 9, no. 6, pp. 2436–2450, Jun. 2016.
[184] K. Liu et al., "LuTan-1: An innovative L-band spaceborne SAR mission," in *Proc. 14th Eur. Conf. Synth. Aperture Radar (EUSAR)*, Leipzig, Germany, Jul. 2022, pp. 1–5.
[185] P. López-Dekker et al., "The harmony mission: End of phase-0 science overview," in *Proc. IEEE Int. Geosci. Remote Sens. Symp. IGARSS*, Brussels, Belgium, Jul. 2021, pp. 7752–7755.
[186] J. Mittermayer et al., "MirrorSAR: An HRWS add-on for single-pass multi-baseline SAR interferometry," *IEEE Trans. Geosci. Remote Sens.*, vol. 60, pp. 1–18, 2021.
[187] V. Pulcino et al., "PLATiNO-1 mission: A compact X-band monostatic and bistatic SAR," in *Proc. 75th Int. Astron. Congr. (IAC)*, Milan, Italy, 2024, pp. 1–11.
[188] Y. Deng et al., "Hongtu-1: The first spaceborne single-pass multibaseline SAR interferometry mission," *IEEE Trans. Geosci. Remote Sens.*, vol. 63, 2025, Art. no. 5202518.
[189] U. Wegmüller, C. Magnard, and O. Frey, "Assessment of Hongtu-1 multi-static X-band SAR constellation interferometry," *Remote Sens.*, vol. 16, no. 19, p. 3600, Sep. 2024.
[190] *EoPortal: Earth Observation Missions*. Accessed: Mar. 31, 2025. [Online]. Available: https://www.eoportal.org/
[191] S. Singh, R. K. Tiwari, V. Sood, R. Kaur, and S. Prashar, "The legacy of scatterometers: Review of applications and perspective," *IEEE Geosci. Remote Sens. Mag.*, vol. 10, no. 2, pp. 39–65, Jun. 2022.
[192] K. Tomiyasu and J. L. Pacelli, "Synthetic aperture radar imaging from an inclined geosynchronous orbit," *IEEE Trans. Geosci. Remote Sens.*, vol. GRS-21, no. 3, pp. 324–329, Jul. 1983.
[193] J. Ruiz Rodon, A. Broquetas, A. Monti Guarnieri, and F. Rocca, "Geosynchronous SAR focusing with atmospheric phase screen retrieval and compensation," *IEEE Trans. Geosci. Remote Sens.*, vol. 51, no. 8, pp. 4397–4404, Aug. 2013.
[194] S. Hobbs, C. Mitchell, B. Forte, R. Holley, B. Snapir, and P. Whittaker, "System design for geosynchronous synthetic aperture radar missions," *IEEE Trans. Geosci. Remote Sens.*, vol. 52, no. 12, pp. 7750–7763, Dec. 2014.
[195] D. Entekhabi et al., "The soil moisture active passive (SMAP) mission," *Proc. IEEE*, vol. 98, no. 5, pp. 704–716, May 2010.
[196] X. Chen, Z. Chen, Y. Li, C. Hu, X. Dong, and S. Hobbs, "Improving 2-D resolution in geosynchronous SAR via spatial spectrum synthesis: Method and verification," *IEEE J. Sel. Topics Appl. Earth Observ. Remote Sens.*, vol. 17, pp. 5847–5863, 2024.
[197] OSCAR. *Observing Systems Capability Analysis and Review Tool: Ludi Tance 4 01A*. Accessed: Mar. 30, 2025. [Online]. Available: https://space.oscar.wmo.int/satellites/view/ludi_tance_4_01a

ABOUT THE AUTHORS

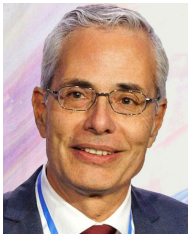

Alberto Moreira (Fellow, IEEE) received the bachelor's and master's degrees in electrical engineering from the Aeronautical Technological Institute (ITA), São José dos Campos, Brazil, in 1984 and 1986, respectively, and the Ph.D. degree (honors) from the Technical University of Munich, Munich, Germany, in 1993.

From 1996 to 2001, he was the Head of the Synthetic Aperture Radar (SAR) Technology Department, German Aerospace Center (DLR), Oberpfaffenhofen, Weßling, Germany. Under his leadership, the DLR airborne SAR system has been upgraded to operate in innovative imaging modes like polarimetric SAR interferometry, tomography, and holography. Since 2001, he has been the Director of the Microwaves and Radar Institute, DLR, and also a Professor with Karlsruhe Institute of Technology (KIT), Karlsruhe, Germany, in the field of microwave remote sensing. His DLR's Institute contributes to several scientific programs and projects for spaceborne SAR missions like TerraSAR-X, TanDEM-X, SAR-Lupe and SARah, Kompsat-6, PAZ, Sentinel-1, BIOMASS, ROSE-L, Harmony, Sentinel-1 NG, EnVision, and VERITAS. The mission TanDEM-X, led by his Institute, has generated a global, high-resolution digital elevation model of the Earth with unprecedented accuracy. He is the Initiator and a Principal Investigator (PI) of this mission. He has authored or co-authored more than 500 publications in international conferences and journals, and nine book chapters, and holds more than 45 patent grants in the radar and antenna field.

Prof. Moreira was a recipient of several international awards including the IEEE Aerospace and Electronic Systems Society (AESS) Fred Nathanson Award in 1999, the IEEE Kiyo Tomiyasu Technical Field Award in 2007, IEEE W. R. G. Baker Award from the IEEE Board of Directors in 2012, the IEEE Geoscience and Remote Sensing Society (GRSS) Distinguished Achievement Award in 2014, and the IEEE Dennis J. Picard Medal for Radar Technologies and Applications in 2023. He and his colleagues received the GRSS transactions prize paper awards in 1997, 2001, and 2007, and the GRSS Letters Prize Paper Award in 2015 and 2017. He has served as the President for the IEEE GRSS in 2010, the General Co-Chair for IGARSS in 2012, the General Chair for EUSAR in 2006, and the Technical Chair for EUSAR 2000. He was the Founder and the Chair of the GRSS German Chapter from 2003 to 2008, served/has been

serving as an Associate Editor for IEEE Geoscience and Remote Sensing Letters from 2003 to 2007 and IEEE Transactions on Geoscience and Remote Sensing since 2005, and served as the Chair for the Major Awards of GRSS from 2017 to 2025. He has served as a member for the ESA Mission Advisory Groups of ENVISAT/ASAR, Sentinel-1, and EnVision, and is currently serving as a member for Hydroterra+.

Gerhard Krieger (Fellow, IEEE) received the Dipl.-Ing. (M.S.) and Dr.-Ing. (Ph.D.) (honors) degrees in electrical and communication engineering from the Technical University of Munich, Munich, Germany, in 1992 and 1999, respectively.

From 1992 to 1999, he was with the Ludwig Maximilian University of Munich, Munich, where he conducted multidisciplinary research on neuronal modeling and nonlinear information processing in biological and technical vision systems. Since 1999, he has been with the Microwaves and Radar Institute, German Aerospace Center (DLR), Oberpfaffenhofen, Weßling, Germany, where he started as a Research Associate, developing signal processing algorithms for a novel forward-looking radar system employing digital beamforming on receive. From 2001 to 2007, he led the New SAR Missions Group, which pioneered the development of advanced bistatic and multistatic radar systems, such as TanDEM-X, as well as innovative multichannel SAR techniques and algorithms for high-resolution wide-swath SAR imaging. Since 2008, he has been the Head of the Radar Concepts Department, which currently hosts about 60 scientists focusing on new SAR techniques, missions, and applications. He has been serving as a Mission Engineer for TanDEM-X, and he also made major contributions to the development of the Tandem-L mission concept, where he led the Phase-0 and Phase-A studies. Since 2019, he has also been holding a professorship at the Friedrich-Alexander University of Erlangen–Nuremberg, Erlangen, Germany. He has authored or co-authored more than 150 peer-reviewed journal articles, nine invited book chapters, about 600 conference papers, and more than 40 patents.

Prof. Krieger has been an Associate Editor for IEEE Transactions on Geoscience and Remote Sensing since 2012. In 2014 and 2024, he served as the Technical Program Chair for European Conference on Synthetic Aperture Radar and also a Guest Editor for IEEE Journal of Selected Topics in Applied Earth Observations and Remote Sensing in 2014. He and his students received more than 40 accolades and best paper awards from international journals and conferences.

Michelangelo Villano (Senior Member, IEEE) received the B.Sc. and M.Sc. degrees (honors) in telecommunication engineering from the Sapienza University of Rome, Rome, Italy, in 2006 and 2008, respectively, and the Ph.D. degree (honors) in electrical engineering and information technology from Karlsruhe Institute of Technology, Karlsruhe, Germany, in 2016.

From 2008 to 2009, he was a Young Graduate Trainee with European Space Research and Technology Center, European Space Agency, Noordwijk, The Netherlands, where he developed processing algorithms for ice sounding radar. Since 2009, he has been with German Aerospace Center (DLR), Microwaves and Radar Institute, Weßling, Germany, where he developed the staggered synthetic aperture radar (SAR) acquisition mode. Since 2019, he has been the Head of the NewSpace SAR Research Group, where he leads the development of cost-effective and multistatic SAR concepts for frequent and enhanced Earth monitoring. In 2017, he was a Visiting Research Scientist with the Communications, Tracking, and Radar Division, NASA Jet Propulsion Laboratory, Pasadena, CA, USA, where he adapted the staggered SAR mode to the NASA-ISRO SAR (NISAR) mission. Since 2019, he has also been a Lecturer with Ulm University, Ulm, Germany. He has authored or co-authored over 40 peer-reviewed journal articles, a book chapter, and over 100 articles in international conference or workshop proceedings. He holds 13 patents in the field of SAR.

Dr. Villano was a recipient of the First Place Student Paper Award at European Conference on Synthetic Aperture Radar (EUSAR), Berlin, Germany, in 2014, the Institute of Electrical and Electronics Engineers (IEEE) Geoscience and Remote Sensing Society (GRSS) Letters Prize Paper Award in 2015 and 2017, the Student Paper Award at the Asia–Pacific Conference on Synthetic Aperture Radar, Marina Bay Sands, Singapore, in 2015, the DLR Science Award in 2016 and 2023, the Award as Young Scientist (now Fellow) of the Foundation Werner von Siemens Ring in 2017, the Information Technology Society (ITG) Dissertation Award in 2017, and the Best Paper Award at German Microwave Conference 2019. In 2022, he was awarded the Starting Grant by European Research Council (ERC). He is the Co-Chair of the Working Group on "Active Microwave: Radar and SAR" of the IEEE GRSS's Technical Committee on Instrumentation and Future Technologies. He is a Distinguished Lecturer of IEEE GRSS for the term 2025–2026. He serves as an Associate Editor for IEEE Transactions on Geoscience and Remote Sensing. He served as a Technical Program Chair for the EUSAR 2024.

Marwan Younis (Fellow, IEEE) received the B.Sc. degree in electrical engineering from the University of Baghdad, Baghdad, Iraq, in 1992, and the Dipl.-Ing. (M.Sc.) and Dr.-Ing. (Ph.D.) degrees in electrical engineering from Universität Karlsruhe (TH), Karlsruhe, Germany, in 1997 and 2004, respectively.

In 1996, he was an Intern with the Jet Propulsion Laboratory (JPL), Pasadena, CA, USA, where he spent research sabbaticals in 2013 and 2019. From 1998 to 2004, he was a Research Scientist with the Institut für Höchstfrequenztechnik und Elektronik, Universität Karlsruhe. Since 2005, he has been with the Microwaves and Radar Institute, German Aerospace Center (DLR), Oberpfaffenhofen, Weßling, Germany. He is currently the Head of the Synthetic Aperture Radar (SAR) Techniques Group, DLR, and also a Professor of spaceborne radar systems with Karlsruhe Institute of Technology (KIT), Karlsruhe. He is a DLR Senior Scientist. He has authored or co-authored about 200 conference papers and 50 reviewed publications, and holds five patents. His research fields include SAR systems and techniques, MIMO SAR, digital beamforming, SAR performance, calibration, and antennas.

Dr. Younis received the Hermann-Billing Award for his Ph.D. thesis in 2005. He is an active member of GRSS. He served GRSS AdCom from 2018 to 2020. He chaired the Instrumentation and Future Technologies GRSS Technical Committee. He is a reviewer of IEEE publications and was an Associate Editor of IEEE Geoscience and Remote Sensing Letters from 2012 to 2019.

Pau Prats-Iraola (Fellow, IEEE) was born in Madrid, Spain, in 1977. He received the Ingeniero and Ph.D. degrees in telecommunications engineering from the Universitat Politècnica de Catalunya (UPC), Barcelona, Spain, in 2001 and 2006, respectively.

In 2001, he was a Research Assistant with the Institute of Geomatics, Barcelona. In 2002, he was with the Department of Signal Theory and Communications, UPC, where he worked in the field of airborne repeat-pass interferometry and airborne differential synthetic aperture radar (SAR) interferometry. From December 2002 to August 2006, he was an Assistant Professor with the Department of Telecommunications and Systems Engineering, Universitat Autònoma de Barcelona, Barcelona. In 2006, he joined the Microwaves and Radar Institute, German Aerospace Center (DLR), Weßling, Germany, where he has been the Head of the Multimodal Algorithms Group since 2009. He is the Responsible and Main Developer of the TanDEM-X Interferometric (TAXI) processor, an end-to-end processing chain for data acquired by the TerraSAR-X and TanDEM-X satellites, which has been used to demonstrate novel SAR acquisition modes and techniques. He is currently involved in the design and implementation of the ground processor prototypes and end-to-end simulators of ESA's BIOMASS, ROSE-L, and Harmony missions. His research interests include high-resolution airborne/spaceborne monostatic/bistatic SAR processing, SAR interferometry, advanced interferometric acquisition modes, persistent scatterer interferometry (PSI), SAR tomography, and end-to-end SAR simulation. He has co-authored more than 70 peer-reviewed journal articles in these fields.

Manfred Zink received the Dipl.-Ing. degree in physics from the Technical University of Graz, Graz, Austria, in 1987, and the Dr.-Ing. degree in aerospace engineering and geodesy from the University of Stuttgart, Stuttgart, Germany, in 1993.

In 1988, he joined the Microwave and Radar Institute, German Aerospace Center (DLR), Weßling, Germany. He has pioneered calibration techniques for both air and spaceborne synthetic aperture radar (SAR) sensors and was responsible for building up the Oberpfaffenhofen calibration site. From 2000 to 2005, he was with European Space Agency (ESA), Noordwijk, The Netherlands, and was responsible for the calibration/validation of the ASAR onboard ENVISAT. In 2005, he returned to the Microwaves and Radar Institute, DLR, where he is currently heading the Satellite SAR Systems Department. From 2006 to 2015, he led the TanDEM-X Ground Segment Project.

Dr. Zink was the General Chair of European SAR Conference (EUSAR) in 2014 and 2024.